Mathematical Biosciences 378 (2024) 109321

Contents lists available at ScienceDirect

Mathematical Biosciences

journal homepage: www.elsevier.com/locate/mbs

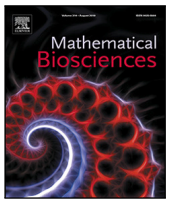

Original Research Article

A metapopulation model with exit screening measure for the 2014–2016 West Africa Ebola virus outbreak

Arsène Jaurès Ouemba Tassé [a,b], Berge Tsanou [b,c,d,e], Jean Louis Woukeng [b], Jean M-S Lubuma [a,*]

[a] School of Computer Science and Applied Mathematics, University of the Witwatersrand, Johannesburg, South Africa
[b] Department of Mathematics and Computer Science, University of Dschang, Cameroon
[c] Department of Mathematics and Applied Mathematics, University of Pretoria, South Africa
[d] LIRIMA-EPITAG, University of Yaounde I, Yaounde, Cameroon
[e] IRD UMMISCO, Sorbonne University, F-93143, Bondy, France

ARTICLE INFO

Keywords:
Ebola
Exit & entry screenings
Global asymptotic stability
Positive frontier equilibria
Nonstandard finite difference schemes

ABSTRACT

We construct a new metapopulation model for the transmission dynamics and control of the Ebola Virus Disease (EVD) in an environment characterized by considerable migrations and travels of people. It is an extended SEIR model modified by the addition of Quarantine and Isolated compartments to account for travelers who undergo the exit screening. The model is well-fitted by using the reported cases from the neighboring countries Guinea, Liberia and Sierra Leone where the 2014–2016 Ebola outbreak simultaneously arose. We show that the unique disease-free equilibrium (DFE) of the model is unstable or locally asymptotically stable (LAS) depending on whether the control reproduction number is larger or less than unity. In the latter case, we prove that the DFE is globally asymptotically stable (GAS) provided that the exit screening is 100% negative. We also prove the GAS of the DFE by introducing more explicit thresholds, thanks to which the existence of at least one boundary equilibrium is established. We design two new nonstandard finite difference (NSFD) schemes, which preserve the dynamics of the continuous model. Numerical simulations that support the theory highlight that exit screening is useful to mitigate the infection. They also suggest that the disease is controlled or the explicit threshold is less than unity provided that the migration and the exit screening parameters are above a critical value.

1. Introduction

The first cases of Ebola Virus Disease (EVD) were reported simultaneously in 1976 in Sudan, now the South Sudan, and in Zaire, now the Democratic Republic of Congo [1]. Since then, the tropical region of Sub-Saharan Africa has experienced the recurrence of 29 outbreaks of which the 2014–2016 West Africa EVD is the largest and severest. It had a significant impact on the world with a total of 28,616 cases and 11,310 deaths [2,3]. Apart from the usual challenges associated with Ebola outbreaks, the 2014–2016 one came with an additional serious challenge. Namely, it arose in three different countries (*viz.* Guinea, Liberia, and Sierra Leone) to and from which migrations and travels of people by road and air were considerable [4–7]. For a better understanding, we provide the narrative below. Contrary to all the previous EVD outbreaks, which were mainly confined in small villages, the 2014–2016 one started in a Guinean village near Guéckédou, moved to some towns and quickly spread first to Liberia and Sierra Leone [3] and later to Mali, Nigeria, Senegal [8,9], due to migrations and travels. According to [4], even at the peak of the 2014–2016 outbreak, many flights were registered from Guinea, Liberia and Sierra Leone to any destination in the world.

WHO recommended the exit screening of travelers at international airports, seaports and major land crossings in the three most affected countries to prevent cross-border transmission of EVD [10–12]. Note that the exit screening is defined as a public health intervention aiming at identifying persons with possible symptoms of a disease or who had a risk of exposure to a disease, in order to prevent them from traveling [12,13]. However, this preventive measure failed to fully confine the EVD because some infected people escaped and caused the exportation of Ebola viruses to other countries such as Spain, the United Kingdom, USA, Mali, Senegal, and Nigeria [3,8,10,14,15]. Understanding the impact of the migrations and travels of people outside the initially afflicted West Africa region on the international spread of EVD is of paramount importance to inform public health interventions. Mathematical modeling has proven for centuries to be a reliable tool to analyze the transmission dynamics of infectious diseases, and to

* Corresponding author.
E-mail address: jean.lubuma@wits.ac.za (J.M.-S. Lubuma).

https://doi.org/10.1016/j.mbs.2024.109321
Received 28 May 2024; Received in revised form 12 October 2024; Accepted 18 October 2024
Available online 29 October 2024

provide recommendations that help to mitigate/contain infectious diseases spreading [16]. This is the main aim of this study.

Since the 2014–2016 EVD outbreak, an outfit of mathematical models have been developed to understand its expansion. A large number of these models assessed the efficiency of control strategies such as quarantine, isolation, vaccination, contact tracing, media coverage [9,17–20], while only few were devoted to the influence of emigration/migration on the spatial spread of EVD [15,21,22]. In [21], for instance, the authors evaluate the efficiency of travel restriction as a control strategy of Ebola in a two-patch model that takes into account the time residents of one patch spend in the other. They showed that reducing the movement between high and low risk regions may have a deleterious influence on the overall level of infection in the total population. The mathematical model in [22] captured the movements of people by only allowing susceptible and latent individuals to travel and by implementing some control measures. The model, utilized to estimate the final magnitude of West Africa EVD outbreak, gave figures close to the exact total numbers of 28,616 cases and 11,310 deaths [3]. In [15], a multi-region model describing the dynamics of population of different geographical areas was proposed, and the utility of travel-blocking at the borders was assessed. The findings there are a bit controversial in that an epidemic region where travel blocking was implemented experienced a higher peak value of infected individuals than in the absence of this intervention. Though the above-mentioned works helped to understand the spread of the EVD, they did not consider the importance of screening travelers at exit borders. As far as the incorporation of entry/exit screening in disease modeling is concerned, many works have been done for other infectious diseases such as mosquito-borne ones and SARS [13,23].

To the best knowledge of the authors, the exit & entry screening interventions, which should be highly relevant for the EVD, has not been investigated from the mathematical modeling perspective. This work aims to fill this gap in line with the recommendation of WHO [12] to implement the exit screening for the 2014–2016 West Africa EVD outbreak. More precisely:

- We construct and analyze a new metapopulation model in which the exit screening, quarantine and isolation are incorporated. The model is parameterized and calibrated using real data from the 2014–2016 outbreak.
- We carry out a quantitative, qualitative and computational analysis. Regarding the latter aspect, we construct two new nonstandard finite difference schemes (NSFD), which are dynamically consistent with respect to the continuous patchy model [24,25].

The rest of the paper is structured as follows: In Section 2, the model with exit screening is formulated. Section 3 deals with the validation of this model. In Section 4, we provide the quantitative and qualitative analysis. Based on two newly developed NSFD schemes, we study numerically, in Section 5, the behavior of the model including the impact of the exit screening and migration rates. In the same section and associated appendix, we carry out the global sensitivity analysis and use it to determine the most influential parameters that drive the dynamics of EVD. In Section 6, we briefly present a more general metapopulation model with exit & entry screening. Section 7 is about concluding remarks (including how our findings fit in the literature), some recommendations, and planned future research work.

2. Model formulation

The models proposed in this work involve the concepts, quarantine and isolation, of public health interventions whose definitions and clarifications given in [26,27] will shortly be recalled. Such explanations are relevant considering the confusion observed in several works. The definition of isolation is straightforward. It is a measure to separate sick people with a contagious disease from those who are not sick [26,27].

A discussion on quarantine modeling is available in [28], where the underlying definition of quarantine is the temporary removal of susceptible individuals who are feared to have been exposed to a communicable disease. This definition implies that in the majority of the quarantine models in the literature, the term "quarantine" was incorrectly used, as highlighted in [28]. In particular, we mention the works [29–32] where only infected individuals were quarantined, with the aim to simplify the model [31,33,34].

Putting this definition in the 'assumed perfect' quarantined modeling process described in [35], it is explained through an adjusted quarantined model in [28] that the quarantined individuals are isolated if they show clinical symptoms of the disease at the end of the quarantine period. If they do not show such symptoms, they return to the susceptible (and actively-mixing) population and they follow a progression of the disease transmission that is parallel to that of non-quarantined susceptible individuals.

In this work, we adopt the epidemiological definition of quarantine whereby it is an intervention that separates and restricts the movement of people who were exposed to a contagious disease to see if they become sick. These people may have been exposed to the disease and do not know it, or they may have the disease but do not show clinical symptoms [26,27]. Hence, apart from the temporarily removed susceptible individuals due to the fear of being exposed to the disease, our quarantine compartment contains exposed and other individuals as stated in the above definition. This enables us to simplify the study by assuming that, unlike [28,35], there is no parallel progression of the two subgroups of quarantined and non-quarantined individuals in the transmission of the disease (the parallel progression will be considered in the general model presented in Section 6). In the current work, the focus is on positively screened travelers who are placed in quarantine in the sense defined above. This is done in accordance with the exit screening guidance given in [12].

2.1. Main assumptions

We build a metapopulation model with patches represented by countries. We take into account the exit screening intervention and consider the following main assumptions:

A1. Only susceptible and latently infected individuals can migrate/move between different patches. Justifications for this assumption include the following: (a) The Ebola virus is a highly virulent pathogen, which gives rise generally to a severe disease [36]. Thus, symptomatic infected individuals are generally unable to travel [22]; (b) The Ebola-deceased individuals are highly contagious and should therefore be buried quickly; (c) Individuals who recover from EVD remain infectious for several months and suffer from several complications such as tiredness, headaches, muscle and joint pains, eye and vision problems, stomach pain and memory loss [37]. Thus, the survivors of EVD continue to receive healthcare or attention in the patch where they have recovered.

A2. Susceptible individuals who intend to travel will be quarantined.

A3. Positively screened travelers are properly isolated to stop their transmission. Some of the isolated people can still travel, after a negative laboratory test, or cancel their trip due to delay. The assumption of isolation is made to simplify the model description. It is achievable once health workers in isolation centers wear appropriate protective clothes to take care of patients [18].

A4. Positively screened travelers who die after a positive diagnosis are safely buried by a well-trained personnel and do not transmit the disease. In fact, it is generally when the corpses are manipulated during mourning, funerals and traditional beliefs that the Ebola-deceased individuals transmit EVD.

A5. The rate at which individuals are positively screened at the exit patch is the same, irrespective of their destinations.

Table 1
Variables of the model.

Classes	Description
S_i	Susceptible individuals in patch i who did not undergo screening or who were negatively screened.
E_i	Latent individuals in patch i.
I_i	EVD symptomatic cases in patch i.
D_i	Ebola-death cases in patch i who are not safely buried.
Q_i	Travelers who are quarantined/on hold due to positive screening at the exit borders of patch i.
P_i	Isolated individuals in patch i who failed to travel due to a positive screening, followed by a positive diagnosis at the exit borders.
R_i	Individuals who recover from EVD in patch i.

A6. The recovered individuals are immune during the outbreak. In fact, it is documented that, recovered individuals develop antibodies that last for at least 10 years [18,37].

A7. Infected individuals will recover or die. Those who die outside isolation centers remain infectious until they are buried.

A8. During the screening process, many susceptible individuals who show flu-and/or malaria-like symptoms can be wrongly positively screened as EVD-infected individuals.

A9. All the individuals positively screened in a patch are sent into the same compartment. This assumption is motivated by the fact that susceptible and latent individuals are apparently not different.

2.2. Model variables

Considering the above assumptions, we choose the model variables as described below. Let $n > 1$ be an integer that represents the number of patches. For each patch $i = 1, 2, \dots, n$, we divide the total population $N_i = N_i(t)$ at time t into seven mutually disjoint compartments: $S_i = S_i(t)$, $E_i = E_i(t)$, $I_i = I_i(t)$, $D_i = D_i(t)$, $Q_i = Q_i(t)$, $P_i = P_i(t)$ and $R_i = R_i(t)$ defined in Table 1. The status of individuals in Q_i is to be travelers (from S_i and E_i) who are positively screened at the exit borders. The replenishment of P_i from Q_i results from a positive diagnosis.

It is convenient to clarify at this stage the main notation we will use throughout this paper. There are so many notation that we will occasionally deviate from the standard convention. Apart from the total population, N_i, we denote by $H_i = H_i(t)$ the total population of individuals who are alive in patch i. Thus,

$$H_i = S_i + E_i + I_i + Q_i + P_i + R_i \text{ and } N_i = H_i + D_i. \tag{2.1}$$

We will denote the sums on all patches by bold uppercase letters. Hence

$$\mathbf{H} = \sum_{i=1}^{n} H_i,\ \mathbf{D} = \sum_{i=1}^{n} D_i \text{ and } \mathbf{N} = \mathbf{H} + \mathbf{D}. \tag{2.2}$$

Given a compartment in patch i, the initial letter/acronym of that compartment will denote the vector function having as components the associated compartments of the n patches. Hence

$$S = (S_1, S_2, \dots, S_n). \tag{2.3}$$

Furthermore, a calligraphic letter such as $\mathcal{X}$ denotes the $7n$-vector-function given by

$$\mathcal{X} = (S, E, I, D, Q, P, R). \tag{2.4}$$

2.3. Derivation of model equations

For any patch i, we assume a constant recruitment, Λ_i, through births in the susceptible population, S_i, and we denote by μ_i the natural mortality rate of all individuals in patch i. EVD is contracted by contact with infectious individuals and manipulation of Ebola-deceased individuals. For the latter channel of infection, some authors used the mass action principle [24,38,39]. Here, we follow [21,28,40,41] and use the standard incidence for both routes of transmission. Hence, the force of infection, λ_i, in patch i is

$$\lambda_i \equiv \lambda_i(t) := \frac{\beta_i(I_i + \nu_i D_i)}{N_i} \tag{2.5}$$

where β_i is the effective transmission rate per unit time of EVD, due to contacts with the infected cases in the compartments I_i, and ν_i is the modification parameter of the infectiousness of the Ebola-deceased individuals.

The susceptible individuals in patch i plan to travel to patch j at the rate a_{ji}. Since EVD has many similar symptoms to those of flu, cholera, typhoid fever, and malaria [42,43], some positively screened people at the exit border of a patch may rather suffer from the latter diseases (see Assumption A8). Let η_i^S be the fraction of susceptible individuals in the S_i compartment who are positively screened at the exit border of patch i. These individuals are placed in quarantine in the Q_i compartment. Their fate is as described in Assumption 3. Let υ_i be the exit rate from the compartment Q_i by any means different from death. We define $\phi_i(S_i, E_i)\upsilon_i$ as the fraction of quarantined individuals who are positively diagnosed. In view of the homogeneous mixing of individuals in the Q_i compartment, we take $\phi_i \equiv \phi_i(S_i, E_i) = E_i/(S_i+E_i)$ i.e the probability for a quarantined individual to be infected, though for simplicity several authors adopt the exponential distribution of exit from Q_i [28,44,45].

Being negatively diagnosed, the remaining number, $(1 - \phi_i(S_i, E_i))\upsilon_i Q_i$, of tested individuals are reverted to the susceptible compartments in patches. More precisely, among those who leave the Q_i compartment, $(1 - \phi_i(S_i, E_i))\upsilon_i\xi_{ii}Q_i$ cancel their trip (at cancellation rate ξ_{ii}) due to delay and thus return to the compartment S_i, while $(1 - \phi_i(S_i, E_i))\upsilon_i\xi_{ji}Q_i$ leave the patch i to the patch j ($j \neq i$), with ξ_{ji} the rate to travel from the Q_i compartment to the compartment S_j. Altogether, the evolution of susceptible individuals in patch i is governed by the following differential equation:

$$\begin{aligned}\frac{dS_i(t)}{dt} &= \Lambda_i - \lambda_i S_i - \mu_i S_i - \sum_{j=1,j\neq i}^{n} a_{ji}S_i + \sum_{j=1,j\neq i}^{n} a_{ij}(1-\eta_j^S)S_j \\ &\quad + \sum_{j=1}^{n}(1 - \phi_i(S_j, E_j))\upsilon_j\xi_{ij}Q_j.\end{aligned} \tag{2.6}$$

Note that the last sum in Eq. (2.6) (i.e. $j = i$) involves the negatively diagnosed individuals from the Q_i compartment who cancelled their trips. It also includes the contributions of all negatively diagnosed quarantine individuals from Q_j compartments in all the patches $j \neq i$ who traveled to S_i in patch i.

Once infected, the susceptible individuals move to the E_i compartment. These individuals progress to the symptomatic stage at the rate α_i. We assume for the sake of simplicity that the individuals in E_i compartment plan to travel to the patch j at the same rate a_{ji}. However, some of them are stopped from traveling by the exit screening implemented at the border of patch i at the rate η_i^E. Positively screened individuals are quarantined and those negatively screened travel. Thus, E_i is governed by the equation:

$$\frac{dE_i(t)}{dt} = \lambda_i S_i - \mu_i E_i - \alpha_i E_i - \sum_{j=1,j\neq i}^{n} a_{ji}E_i + \sum_{j=1,j\neq i}^{n} a_{ij}(1-\eta_j^E)E_j. \tag{2.7}$$

Due to the exit screening at the border of patch i, there are $a_{ji}\eta_i^S S_i$ and $a_{ji}\eta_i^E E_i$ susceptible and latent individuals of patch i who wanted to travel to patch j but are stopped and quarantined in Q_i. Individuals in quarantine are monitored [19] and undergo laboratory tests at rate υ_i. This gives them a better chance to recover since they are treated at an early stage of the disease [46]. The dynamics of individuals in quarantine is:

$$\frac{dQ_i(t)}{dt} = \sum_{j=1,j\neq i}^{n} a_{ji}\eta_i^E E_i + \sum_{j=1,j\neq i}^{n} a_{ji}\eta_i^S S_i - (\mu_i + \upsilon_i)Q_i. \tag{2.8}$$

Quarantined individuals who are tested positive are isolated (Assumption 3). Unlike those in the I_i compartment, they enjoy special care, being identified early and followed in hospital training.

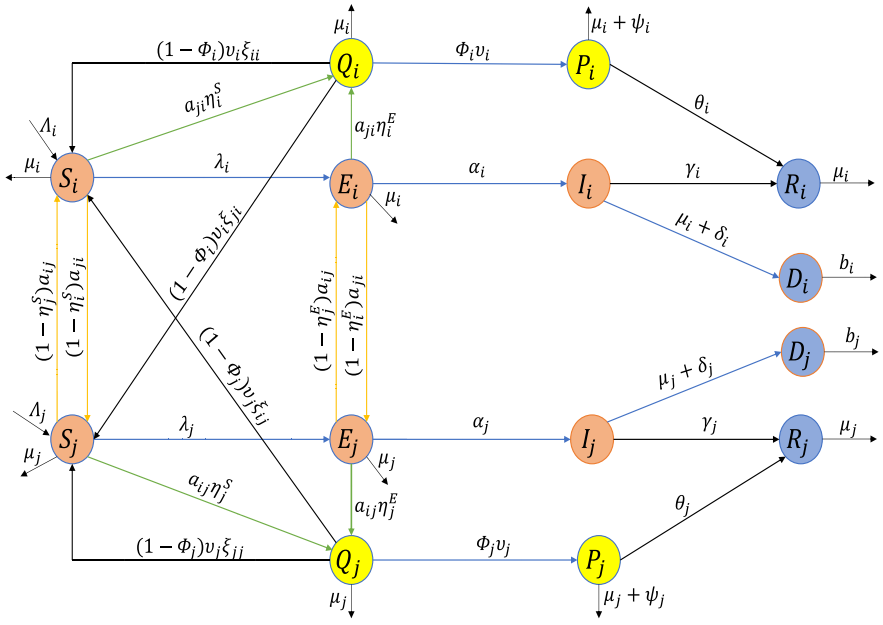

Fig. 1. Flow diagram between two infected patches i and j $(i \neq j)$ for Model (2.13).

In the P_i compartment, an individual can either recover at the rate θ_i or die at the disease-induced death rate ψ_i, apart from natural death at rate μ_i [47,48]. Hence the dynamics of P_i is

$$\frac{dP_i(t)}{dt} = \phi_i(S_i, E_i)\upsilon_i Q_i - (\mu_i + \psi_i + \theta_i)P_i. \tag{2.9}$$

Because of the virulence of the Ebola virus, we can assume that the individuals in the I_i compartment are so sick that they cannot travel. These individuals may recover at the rate γ_i, die naturally at the rate μ_i, or because of the disease at the rate δ_i. Note that the individuals in P_i are managed in the early stage of EVD, contrarily to those of I_i. Thus, both mortality and recovery rates in the P_i and I_i compartments can be different. Taking into account the latent individuals who become symptomatic, the dynamics of the I_i compartment is given by the equation:

$$\frac{dI_i(t)}{dt} = \alpha_i E_i - (\mu_i + \delta_i + \gamma_i)I_i. \tag{2.10}$$

The Ebola-deceased individuals as well as the symptomatic individuals who die by any other causes are infectious since their corporal liquids already contain the virus [47,48]. All these individuals are gathered in the D_i compartment. The individuals in the D_i compartment are buried at the rate b_i. The model for D_i is given by

$$\frac{dD_i(t)}{dt} = (\mu_i + \delta_i)I_i - b_i D_i. \tag{2.11}$$

Individuals who recover from EVD in I_i and P_i compartments move to the R_i compartment. These recovered individuals have some sequelae of the disease; so we may assume that they do not travel because they still require some follow-up. The dynamic of R_i is given by

$$\frac{dR_i(t)}{dt} = \gamma_i I_i + \theta_i P_i - \mu_i R_i. \tag{2.12}$$

Putting everything together, the model parameters and their biological meanings are summarized in Table 2. The flow diagram of the patch model is given on Fig. 1. The associated metapopulation model for n patches reads as follows for $i = 1, 2, \ldots, n$:

$$\begin{cases}
\dfrac{dS_i(t)}{dt} &= \Lambda_i - \lambda_i S_i - \mu_i S_i - \displaystyle\sum_{j=1,j\neq i}^{n} a_{ji}S_i + \sum_{j=1,j\neq i}^{n} a_{ij}(1-\eta_j^S)S_j \\
&\quad + \displaystyle\sum_{j=1}^{n}(1-\phi_j(S_j,E_j))\upsilon_j\xi_{ij}Q_j, \\
\dfrac{dE_i(t)}{dt} &= \lambda_i S_i - \mu_i E_i - \alpha_i E_i - \displaystyle\sum_{j=1,j\neq i}^{n} a_{ji}E_i + \sum_{j=1,j\neq i}^{n} a_{ij}(1-\eta_j^E)E_j, \\
\dfrac{dI_i(t)}{dt} &= \alpha_i E_i - (\mu_i + \delta_i + \gamma_i)I_i, \\
\dfrac{dD_i(t)}{dt} &= (\mu_i + \delta_i)I_i - b_i D_i, \\
\dfrac{dQ_i(t)}{dt} &= \displaystyle\sum_{j=1,j\neq i}^{n} a_{ji}\eta_i^E E_i + \sum_{j=1,j\neq i}^{n} a_{ji}\eta_i^S S_i - (\mu_i + \upsilon_i)Q_i, \\
\dfrac{dP_i(t)}{dt} &= \phi_i(S_i,E_i)\upsilon_i Q_i - (\mu_i + \psi_i + \theta_i)P_i, \\
\dfrac{dR_i(t)}{dt} &= \gamma_i I_i + \theta_i P_i - \mu_i R_i.
\end{cases} \tag{2.13}$$

We obtain the following conservation law by adding the equations in (2.13), excluding the equation of the deaths.

$$\frac{dH_i(t)}{dt} = \Lambda_i - \mu_i H_i - \delta_i I_i - \psi_i P_i. \tag{2.14}$$

Moreover, for Model (2.13) to be epidemiological meaningful, it is necessary to assume that the initial conditions are non-negative such that

$$S_i(0) > 0,\ \forall\, i \in \{1, \ldots, n\},\ \sum_{i=1}^{n}(E_i(0) + I_i(0) + D_i(0)) > 0. \tag{2.15}$$

3. Model validation

To assess the usefulness of the exit screening measure, we restrict this section to $n = 3$ patches corresponding to Guinea, Liberia, and Sierra Leone where the 2014–2016 West Africa Ebola outbreak was more pronounced. The movements between patches being modeled by

Table 2
Parameters of the model.

Parameters	Epidemiological interpretation	Units
a_{ij}	Rate of susceptible/latent individuals of patch j who wish to migrate to patch i.	week^{-1}
μ_i	Natural mortality rate in patch i.	week^{-1}
Λ_i	Constant recruitment of susceptible individuals in patch i.	indiv week^{-1}
β_i	Effective transmission rate of EVD in patch i due to individuals in I_i compartment.	indiv week^{-1}
b_i	Burial rate of Ebola-deceased in patch i.	week^{-1}
γ_i, θ_i	Recovery rate of infected who belong to the I_i, P_i compartment.	week^{-1}
α_i	Exit rate of the E_i compartment to the I_i compartment.	week^{-1}
ν_i	Modification parameter for the infectiousness of the Ebola-deceased.	–
η_i^S	Proportion of susceptible individuals in S_i who are positively screened at the exit border of patch i.	–
η_i^E	Proportion of latent individuals in E_i who are positively screened at the exit border of patch i.	–
δ_i	Mortality rate due to EVD of infected individuals in patch i who belong to the I_i compartment.	week^{-1}
ψ_i	Mortality rate due to EVD of infected in patch i who belong to the P_i compartment.	week^{-1}
υ_i	Exit rate from the Q_i compartment by any means different from the death.	week^{-1}
$\phi_i(S_i, E_i)\upsilon_i$	Fraction of quarantined individuals who are positively diagnosed.	week^{-1}
ξ_{ij}	Rate at which the quarantined who are negatively diagnosed in patch j left patch j to patch i ($j \neq i$).	week^{-1}
ξ_{ii}	Rate at which the quarantined who are negatively diagnosed in patch i cancel their trip.	week^{-1}

Table 3
Estimation of the rates of travel a_{ij} between countries through Eq. (3.1).

Countries $N^o i$	Population T_i	Annual migrant M_{ij} from j to i	Travel rate from j to i
1.Guinea	T_1 = 11,055,429 [52]	M_{12} = 118,353 [5] M_{13} = 226,415 [5]	a_{12} = 0.00054 a_{13} = 0.00063
2.Liberia	T_2 = 4,248,000 [53]	M_{21} = 37,026 [6] M_{23} = 13,165 [6]	a_{21} = 0.000064 a_{23} = 0.000036
3.Sierra Leone	T_3 = 6,964,859 [54]	M_{31} = 61,510 [7] M_{32} = 22,144 [7]	a_{31} = 0.0001 a_{32} = 0.0001

Table 4
Initial values of the variables for Model (2.13).

Countries	E(0)	I(0)	D(0)	Q(0)	P(0)	R(0)	Total
Guinea	330	286	286	286	286	286	1760
Liberia	1319	1060	1060	1060	1060	1060	6619
Sierra Leone	1262	920	920	720	520	520	4862

an exponential distribution, it would be more appropriate to estimate the migration rates as in [49]. However, due to the difficulty of this approach and the lack of relevant data, we use a simple method. Identifying the three countries by the number (i), $i = 1, 2, 3$, the annual number M_{ij} of migrants from a country number j to a country number i is provided in [5–7] as recorded in Table 3. Furthermore, Table 3 is enriched with the weekly number, $M_{ij}/52$ of migrants and the total population T_j of country number j, which in turn gives

$$a_{ij} = \frac{M_{ij}}{52 \times T_j} \tag{3.1}$$

as the travel rate from country number j to country number i. Moreover, for the P_i compartment of isolated or hospitalized individuals, we take the death rates and the recovery rates given in [39,41,50,51] (see Table 5). Parameters found in the literature are gathered in Table 5, while the other parameters are obtained by fitting the model to the reported data.

WHO recommended the exit screening of travelers at the border of these countries on November 06 2014 [12]. We fit Model (2.13) to the cumulative number $C(t)$ of infected recorded in these countries from 07 November 2014 (initial date) to 07 August 2015 (end-date) [55], which corresponds to 40 weeks. According to [56], the dynamics of $C(t)$ is given as $\dot{C} = \sum_{i=1}^{3} \lambda_i S_i$. We utilize the Nonlinear Least Squares fitting method, implemented by "fminsearchbn" function in Matlab Software. The Nonlinear Least Squares method allows the determination of the set of parameters that minimizes the sum of the squares of the differences between the predicted cumulative infected by the model and the observed cumulative cases [57]. The population of Guinea, Liberia and Sierra Leone are assumed to be the number of susceptible individuals in these countries. For the initial number of infected, we split on Table 4 the cumulative initial cases 1760 in Guinea, 6619 in Liberia and 4862 in Sierra Leone in the compartments E, I, D, Q, P and R. Fig. 2 shows excellent fitting between cumulative cases of the Model (2.13) with the values displayed on Table 5.

4. Mathematical analysis

The mathematical analysis of Model (2.13) requires several notation. To those specified in (2.2), (2.3) and (2.4), we add the following. We denote by $\mathrm{diag}(x)$ or $\mathrm{diag}(x_i)_{i=1}^{i=n}$ the $n \times n$ diagonal matrix, whose diagonal entries are the coordinates of the vector $x = (x_1, \ldots, x_n) \in \mathbb{R}^n$. Moreover, we add the notation

$$\begin{aligned}
&\mathbf{\Lambda} = \sum_{i=1}^{n} \Lambda_i;\ \Upsilon = \sum_{i=1}^{n} [(\mu_i + \delta_i)];\ \mu_m = \min_{1\le i\le n} \{\mu_i\};\ j_i = \mu_i b_i k_i (\mu_i + \alpha_i),\\
&\quad k_i = (\mu_i + \delta_i + \gamma_i);\\
&b_m = \min_{1\le i\le n} \{b_i\};\ \mu_M = \max_{1\le i\le n} \{\mu_i + \delta_i + \psi_i\};\\
&\quad \omega_i = \mu_i b_i k_i + \mu_i b_i \alpha_i + \mu_i \alpha_i (\mu_i + \delta_i) + \gamma_i b_i \alpha_i;\\
&a^M = \max_{1\le i\le n} (\beta_i (1 + \nu_i) + \mu_i + \sum_{j=1}^{n} a_{ji});\ \alpha^M = \max_{1\le i\le n} (\mu_i + \alpha_i);\\
&\quad \gamma^M = \max_{1\le i\le n} (\mu_i + \delta_i + \gamma_i);\\
&b^M = \max_{1\le i\le n} (b_i);\ \upsilon^M = \max_{1\le i\le n} (\mu_i + \upsilon_i);\ \theta^M = \max_{1\le i\le n} (\mu_i + \psi_i + \theta_i);\\
&\quad \mu^M = \max_{1\le i\le n} (\mu_i);
\end{aligned} \tag{4.1}$$

Furthermore, considered for all n patches, Model (2.13) can be written in the compact form,

$$\frac{d\mathcal{X}}{dt} = \mathcal{G}(\mathcal{X}), \tag{4.2}$$

Table 5
Parameters values to simulate System (2.13).

Par.	Values	Source	Range	Par.	Values	Source	Range
η_1^E	0.0239	Fitted	0–1	η_2^E	0.0478	Fitted	0–1
μ_1	0.0002	[58]	0–1	υ_1	0.2758	Fitted	0–1
β_1	0.2556	Fitted	0–1	β_2	0.1209	Fitted	0–1
β_3	0.2822	Fitted	0–1	υ_2	0.2565	Fitted	0–1
ν_1	0.9374	Fitted	0–1	ν_2	0.8524	Fitted	0–1
ν_3	0.4044	Fitted	0–1	η_3^S	0.1935	Fitted	0–1
δ_1	0.857	[59]	0–1	δ_2	0.75	[60]	0–1
δ_3	0.5	[50]	0–1	υ_3	0.3173	Fitted	0–1
ψ_1	0.3	[41]	0–1	ψ_2	0.4	[39]	0–1
ψ_3	0.5	[50]	0–1	ξ_{21}	0.2823	Fitted	
ξ_{31}	0.3813	Fitted	0–0.5	ξ_{12}	0.4067	Fitted	0–0.5
ξ_{11}	0.0572	Fitted	0–0.5	ξ_{22}	0.1307	Fitted	0–0.5
ξ_{33}	0.0893	Fitted	0–0.5	η_3^E	0.0578	Fitted	0–1
ξ_{32}	0.0686	Fitted	0–0.5	ξ_{13}	0.8997	Fitted	0–0.5
ξ_{23}	0.2483	Fitted	0–0.5	a_{21}	0.000064	Estimated	0–0.5
a_{31}	0.0001	Estimated	0–0.5	a_{12}	0.00054	Estimated	0–0.5
a_{32}	0.0001	Estimated	0–0.5	a_{13}	0.00063	Estimated	0–0.5
a_{23}	0.000036	Estimated	0–0.5	b_3	0.5	[50]	0–1
b_1	1/2.01	[50]	0–1	b_2	1/4.5	[60]	0–1
γ_1	0.0059	[51]	0–1	γ_2	0.026767	[51]	0–1
θ_1	0.001120	[51]	0–1	θ_2	0.031486	[51]	0–1
θ_3	0.015743	[51]	0–1	γ_3	0.010038	[51]	0–1
η_2^S	0.0299	Fitted	0–1	μ_2	0.0002	[58]	0–1
μ_3	0.0002	[58]	0–1	$\Lambda_i,\ \forall\, i$	0.03703	[61]	0–1
α_1	0.4127	Fitted	0–1	α_2	0.4532	Fitted	0–1
α_3	1.9440	Fitted	0–1	η_1^S	0.8535	Fitted	0–1

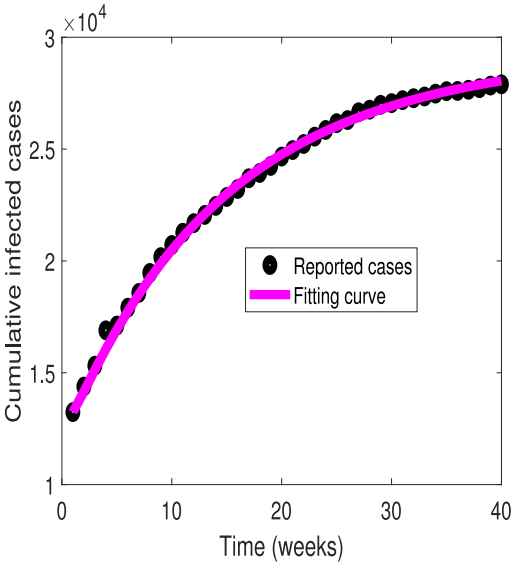

Fig. 2. Curve fitting for Model (2.13) from real data of the 2014–2016 EVD outbreak in Guinea, Liberia, and Sierra Leone [55] from 7 November 2014 to 7 August 2015. The values used for the simulation are in Table 5.

where $\mathcal{X} \equiv \mathcal{X}(t)$, as in (2.4), denotes the solution of the system with right-hand side, $\mathcal{G}$, structured as

$$\mathcal{G}(\mathcal{X}) = (G_{S_1}, \dots, G_{S_n}, F_{E_1}, \dots, G_{E_n}, G_{I_1}, \dots, G_{I_n}, G_{D_1}, \dots, G_{D_n}, G_{Q_1}, \dots, G_{Q_n}, G_{P_1}, \dots, G_{P_n}, G_{R_1}, \dots, G_{R_n})^T, \tag{4.3}$$

where G_{A_i} represents the right-hand side of the equation of the dynamics of the compartment A_i, $A = S, E, I, D, Q, P, R$.

4.1. Well-posedness of the model

The well-posedness of Model (2.13) is given in the next result.

Theorem 4.1. *Model (2.13) is a dynamical system on the following biologically feasible and attractive region:*

$$\Gamma := \left\{ \mathcal{X} = (S, E, I, D, Q, P, R) \in \mathbb{R}_+^{7n} : \mathbf{H} \le \frac{\mathbf{\Lambda}}{\mu_m} \text{ and } \mathbf{D} \le \frac{\mathbf{\Upsilon}\Lambda}{\mu_m b_m} \right\}.$$

Proof. The theorem results from the combination of the four facts below [62].

- Model (4.2) possesses a unique local solution since its right-hand side $\mathcal{F}$ is locally Lipschitz.
- The positive cone $\mathbb{R}_+^{7n}$ is forward invariant with respect to the system. This is obtained by the tangent condition applied to each of the $7n$ hyperplanes that forms the boundary of $\mathbb{R}_+^{7n}$, observing that the unit normal vector to each hyperplane is a vector of the canonical basis of the space $\mathbb{R}^{7n}$ [63,64].
- Any solution $\mathcal{X}(t) = (S(t), E(t), I(t), D(t), Q(t), P(t), R(t)) \in \mathbb{R}_+^{7n}$ of Model (2.13) initiated at a point $\mathcal{X}(0) \in \Gamma$ satisfies *a priori* estimates

$$\mathbf{H}(t) \le \frac{\mathbf{\Lambda}}{\mu_m},\ \forall\, t > 0 \text{ and } \limsup_{t \longrightarrow +\infty} \mathbf{H}(t) \le \frac{\mathbf{\Lambda}}{\mu_m} \tag{4.4}$$

and

$$\mathbf{D}(\mathbf{t}) \le \frac{\mathbf{\Upsilon}\Lambda}{b_m \mu_m},\ \forall\, t > 0 \text{ and } \limsup_{t \longrightarrow +\infty} \mathbf{D}(t) \le \frac{\mathbf{\Upsilon}\Lambda}{b_m \mu_m}. \tag{4.5}$$

Indeed, by adding in (2.13), the equations of individuals who are alive and summing up over all patches the resulting equations as well as those of the Ebola-deceased individuals, we obtain the conservation laws

$$\frac{d\mathbf{H}}{dt} = \sum_{i=1}^{n} [\Lambda_i - \mu_i H_i - \delta_i I_i - \psi_i P_i] \le \mathbf{\Lambda} - \mu_m \mathbf{H} \tag{4.6}$$

and

$$\frac{d\mathbf{D}}{dt} = \sum_{i=1}^{n} [(\mu_i + \delta_i) I_i - b_i D_i] \le \frac{\mathbf{\Upsilon}\Lambda}{\mu_m} - b_m \mathbf{D}. \tag{4.7}$$

The application of Gronwall inequality to (4.6) and (4.7) yields for every $t \ge 0$,

$$\mathbf{H}(t) \le \frac{\mathbf{\Lambda}}{\mu_m} + \left(\mathbf{H}(0) - \frac{\mathbf{\Lambda}}{\mu_m} \right) e^{-\mu_m t} \text{ and } \mathbf{D}(t) \le \frac{\mathbf{\Upsilon}\Lambda}{b_m \mu_m} + \left(\mathbf{D}(0) - \frac{\mathbf{\Upsilon}\Lambda}{b_m \mu_m} \right) e^{-b_m t}, \tag{4.8}$$

from which (4.4) and (4.5) follow.

- The set Γ is attractive. This follows from the second inequalities in (4.4) and (4.5).

4.2. Existence of the disease-free equilibrium

To find an equilibrium point $\mathcal{E}^* \equiv (S^*, E^*, I^*, D^*, Q^*, P^*, R^*) \in \mathbb{R}_+^{7n}$ of System (2.13), we set its right hand side equal to zero. By definition, a disease-free equilibrium (DFE), $\mathcal{E}^*$, is such that the force of infection given in (2.5) and evaluated at $\mathcal{E}^*$ is equal to zero: $\lambda^* = 0$ i.e. $I^* = D^* = 0$. This implies that $E^* = P^* = R^* = 0$. Hence, finding the DFE reduces to solving the following linear system.

$$\begin{cases} \Lambda_i - \mu_i S_i - \sum_{j=1, j\neq i}^{n} a_{ji} S_i + \sum_{j=1, j\neq i}^{n} a_{ij} (1 - \eta_j^S) S_j + \sum_{j=1}^{n} \upsilon_j \xi_{ij} Q_j = 0 \\ \sum_{j=1, j\neq i}^{n} a_{ji} \eta_i^S S_i - (\mu_i + \upsilon_i) Q_i = 0,\ i = 1, 2, \dots, n. \end{cases} \tag{4.9}$$

The System (4.9) takes the matrix form

$$CU = \Pi, \tag{4.10}$$

with $U = (S_1, S_2, \dots, S_n, Q_1, Q_2, \dots, Q_n)^T \equiv (S, Q)^T$, $\Pi = (\Lambda_1, \Lambda_2, \dots, \Lambda_n, 0, \dots, 0)^T$ and C (see Eq. (4.11) in Box I). Since the sum of each column of C is μ_i ($\mu_i > 0$) and all the off-diagonal entries of C are non-positive, C is a non singular M-matrix and $C^{-1} \ge 0$ [65]. Thus, Eq. (4.10)

$$C = \begin{pmatrix} \mu_1 + \sum_{j=2}^{n} a_{j1} & -a_{12}(1-\eta_2^S) & \cdots & -a_{1n}(1-\eta_n^S) & -\upsilon_1\xi_{11} & -\upsilon_2\xi_{12} & \cdots & -\upsilon_n\xi_{1n} \\ -a_{21}(1-\eta_1^S) & \mu_2 + \sum_{j=1,j\neq 2}^{n} a_{j2} & \cdots & -a_{2n}(1-\eta_n^S) & -\upsilon_1\xi_{21} & -\upsilon_2\xi_{22} & \cdots & -\upsilon_n\xi_{2n} \\ \vdots & \vdots & \vdots & \vdots & \vdots & \vdots & \vdots & \\ -a_{n1}(1-\eta_1^S) & -a_{n2}(1-\eta_2^S) & \cdots & \mu_n + \sum_{j=1}^{n-1} a_{jn} & -\upsilon_1\xi_{n1} & -\upsilon_2\xi_{n2} & \cdots & -\upsilon_n\xi_{nn} \\ -\sum_{j=2}^{n} a_{j1}\eta_1^S & 0 & \cdots & 0 & (\mu_1+\upsilon_1) & 0 & \ldots & 0 \\ 0 & -\sum_{j=1,j\neq 2}^{n} a_{j2}\eta_2^S & \cdots & 0 & 0 & (\mu_2+\upsilon_2) & \ldots & 0 \\ \vdots & \vdots & \vdots & \vdots & \vdots & \vdots & \vdots & \\ 0 & 0 & \cdots & -\sum_{j=1}^{n-1} a_{jn}\eta_n^S & 0 & 0 & \cdots & (\mu_n+\upsilon_n) \end{pmatrix} \tag{4.11}$$

Box I.

has a unique positive solution given by $U^0 = (S^0, Q^0)^T = C^{-1}\Pi$. We have established the following result.

Proposition 4.2. *System (2.13) has a unique disease-free equilibrium $\mathcal{E}_0$, given by*

$$\mathcal{E}_0 = (S^0, 0, 0, 0, Q^0, 0, 0). \tag{4.12}$$

The matrix $(a_{ij})_{1\leq i,j\leq n}$ of the rates of migration of susceptible and latent individuals between patches can be irreducible. Practically, this means that, susceptible and latent individuals can travel between any two sets of patches directly or indirectly (e.g nonstop or connecting flights). Indirect travel from patch j to patch i means that there is a sequence $(j_k)_{1\leq k\leq n-2}$ on the set $\{1,\ldots,n\}$ such that there are a direct travels $j \to j_{k-2}$, $j_{k-2} \to j_{k-3}$,..., $j_{k_1} \to i$. This being clarified, we have the following result.

Proposition 4.3. *Assume the matrix $(a_{ij})_{1\leq i,j\leq n}$ is irreducible. If one patch is disease-free and System (2.13) is at equilibrium, then all the patches are disease-free.*

Proof. Without loss of generality, we denote by i the disease-free patch and A_i the set of indices directly connected to the patch i. That is

$$A_i = \{j : a_{ij} > 0,\ j = 1,\ldots,n, j \neq i\}. \tag{4.13}$$

Since System (2.13) is at equilibrium, we have $\dot{E}_i(t) = 0$ and

$$\sum_{j=1,j\neq i}^{n} a_{ij}(1-\eta_j^E)E_j = 0. \tag{4.14}$$

Thus, for all $j \in A_i$, $E_j = 0$. This implies that $I_j = D_j = P_j = R_j = 0$, so that all the patches for which the subscripts belong to A_i are disease-free. If $j \notin A_i$, the fact that the matrix $(a_{ij})_{1\leq i,j\leq n}$ is irreducible proves that there exist $j_1, j_2, \ldots, j_p$ such that, $a_{j_1 j}, a_{j_2 j_1}, \ldots, a_{j_p j_{p-1}}, a_{i j_p} > 0$. Hence $j_p \in A_i$ and thus $E_{j_p} = I_{j_p} = D_{j_p} = P_{j_p} = R_{j_p} = 0$. Similarly, $j_{p-1} \in A_{j_p}$, i.e $E_{j_{p-1}} = I_{j_{p-1}} = D_{j_{p-1}} = P_{j_{p-1}} = R_{j_{p-1}} = 0$. By mathematical induction, one has $j \in A_{j_1}$ and so, $E_j = I_j = D_j = P_j = R_j = 0, \forall j \notin A_i$. Hence all the n patches are disease-free. □

Proposition 4.3 points out that, when the matrix $(a_{ij})_{1\leq i,j\leq n}$ is irreducible, the model does not admit a positive frontier boundary equilibrium. The case where the matrix $(a_{ij})_{1\leq i,j\leq n}$ is reducible is addressed in the next subsection.

4.3. Patch boundary equilibria

In this subsection, we investigate the existence of boundary equilibrium, $\mathcal{E}_0^i$, characterized by the fact that, $\forall\, j = 1,\ldots,n$, $j \neq i$, the patch j is disease-free, while patch i has positive equilibrium:

$$\begin{aligned}\mathcal{E}_0^i \ :=\ & (S_1^0, 0, 0, 0, Q_1^0, 0, 0, \ldots, S_{i-1}^0, 0, 0, 0, Q_{i-1}^0, 0, 0, S_i^*, E_i^*, I_i^*, \\ & D_i^*, Q_i^*, P_i^*, R_i^*, \\ & S_{i+1}^0, 0, 0, 0, Q_{i+1}^0, 0, 0, \ldots, S_n^0, 0, 0, 0, Q_n^0, 0, 0).\end{aligned}$$

Let us fix $k \in \{1,\ldots,n\}$, $k \neq i$. The patch k is disease-free. Thus, at the equilibrium $\mathcal{E}_0^i$, by using the equation of $\dot{E}_i$ one has

$$\sum_{j=1,j\neq k}^{n} a_{kj}(1-\eta_j^E)E_j = 0,$$

which implies that

$$a_{ki}(1-\eta_i^E)E_i^* = 0.$$

Since we find a positive equilibrium, we get

$$a_{ki} = 0,\ \forall\, k \in \{1,\ldots,n\},\ k \neq i.$$

This means that the matrix $(a_{ij})_{1\leq i,j\leq n}$ is reducible.

In this case,

$$\sum_{j=1,j\neq i}^{n} a_{ji} = 0, \quad \sum_{j=1,j\neq i}^{n} a_{ji}\eta_i^E = 0, \quad \sum_{j=1,j\neq i}^{n} a_{ji}\eta_i^S = 0 \tag{4.15}$$

and therefore $Q_i^* = P_i^* = 0$ from System (2.13).

Since $\forall\ j \neq i$, the patch j is disease-free, $\phi_j(S_j, E_j) = 0$. Hence, finding $\mathcal{E}_0^i$ amounts to solving the following system obtained from (2.13)

$$\begin{cases} \Lambda_i - \lambda_i^* S_i^* - \mu_i S_i^* + \sum_{j=1,j\neq i}^{n} a_{ij}(1-\eta_j^S)S_j^0 + \sum_{j=1,j\neq i}^{n} \upsilon_j\xi_{ij}Q_j^0 = 0, \\ \lambda_i^* S_i^* - \mu_i E_i^* - \alpha_i E_i^* = 0, \\ \alpha_i E_i^* - k_i I_i^* = 0, \\ (\mu_i + \delta_i)I_i^* - b_i D_i^* = 0, \\ \gamma_i I_i^* - \mu_i R_i^* = 0. \end{cases} \tag{4.16}$$

Simple computations lead to

$$E_i^* = \frac{\lambda_i^* S_i^*}{\mu_i + \alpha_i}, \quad I_i^* = \frac{\alpha_i \lambda_i^* S_i^*}{k_i(\mu_i + \alpha_i)}, \quad D_i^* = \frac{(\mu_i + \delta_i)\alpha_i \lambda_i^* S_i^*}{b_i k_i(\mu_i + \alpha_i)},$$
$$R_i^* = \frac{\gamma_i \alpha_i \lambda_i^* S_i^*}{\mu_i k_i(\mu_i + \alpha_i)}$$
$$S_i^* = \frac{\Lambda_i + \sum_{j=1, j\neq i}^n a_{ij}(1-\eta_j^S) S_j^0 + \sum_{j=1, j\neq i}^n \upsilon_j \xi_{ij} Q_j^0}{(\lambda_i^* + \mu_i)}$$

Moreover, one can easily get that

$$N_i^* = \frac{S_i^*(j_i + \omega_i \lambda_i^*)}{b_i k_i \mu_i(\mu_i + \alpha_i)} \text{ and } \lambda_i^* = \frac{\mu_i \beta_i \left[b_i \alpha_i + \nu_i \alpha_i(\mu_i + \delta_i)\right] \lambda_i^* S_i^*}{S_i^*(j_i + \omega_i \lambda_i^*)}$$

Therefore,

$$\lambda_i^* = \frac{j_i}{\omega_i}\left(\mathcal{P}_i^0 - 1\right), \text{ where } \mathcal{P}_i^0 = \frac{\beta_i \left[b_i \alpha_i + \nu_i \alpha_i(\mu_i + \delta_i)\right]}{b_i k_i(\mu_i + \alpha_i)}.$$

This proves that the frontier equilibrium $\mathcal{E}_0^i$ exists if and only if $\mathcal{P}_i^0 > 1$, as comprehensively stated in the next result.

Proposition 4.4. *Assume that the matrix $(a_{ij})_{1\leq i,j\leq n}$ is reducible. Then Model (2.13) admits p boundary equilibria E_0^i, whenever $\mathcal{P}_{l_i}^0 > 1, l_1, l_2 \ldots, l_p \in \{1, \ldots, n\}$, $i = 1, \ldots, p$. Otherwise, the disease-free equilibrium $\mathcal{E}_0$ is the unique boundary equilibrium for Model (2.13) if $\forall\, i = 1, \ldots, n$, $\mathcal{P}_i^0 \leq 1$.*

4.4. Control reproduction number and stability of the disease-free equilibrium

The control reproduction number for Model (2.13) is defined as the average number of secondary infections produced by an index case introduced in the population during its entire infectious period when the exit screening is implemented. The terminology control reproduction number is preferred to the usual terminology of basic reproduction number because, we are considering the average number of secondary infections introduced rather in a "reduced" (by the quarantine process) population of susceptible instead of the entire population. To compute this number, we use the next generation matrix approach presented in [66].

The infected classes for our model are E, I and D. The matrices, F, of appearance of new infections and, V, of transition are

$$F = \begin{pmatrix} 0 & \vdots & F_{12} & \vdots & F_{13} \\ \cdots & & \cdots & & \cdots \\ 0 & \vdots & 0 & \vdots & 0 \\ \cdots & & \cdots & & \cdots \\ 0 & \vdots & 0 & \vdots & 0 \end{pmatrix} \text{ and } V = \begin{pmatrix} V_{11} & \vdots & 0 & \vdots & 0 \\ \cdots & & \cdots & & \cdots \\ V_{21} & \vdots & V_{22} & \vdots & 0 \\ \cdots & & \cdots & & \cdots \\ 0 & \vdots & V_{32} & \vdots & V_{33} \end{pmatrix} \tag{4.17}$$

where $F_{12}, F_{13}, V_{21}, V_{32}, V_{22}, V_{11}$ and V_{33} are $n\times n$ block matrices defined by

$$\begin{aligned} &F_{12} = \text{diag}(\beta_i \tfrac{S_i^0}{N_i^0})_{i=1}^{i=n},\ F_{13} = \text{diag}(\beta_i \nu_i \tfrac{S_i^0}{N_i^0})_{i=1}^{i=n},\ V_{21} = \text{diag}(-\alpha_i)_{i=1}^{i=n}, \\ &V_{32} = \text{diag}(-\mu_i - \delta_i)_{i=1}^{i=n}, \\ &V_{22} = \text{diag}(\mu_i + \delta_i + \gamma_i,)_{i=1}^{i=n},\ V_{33} = \text{diag}(b_i)_{i=1}^{i=n}, \\ &V_{11} = \text{diag}(\sum_{j\neq i}^n a_{ji} + \mu_i + \alpha_i)_{i=1}^{i=n} - M^E, \end{aligned} \tag{4.18}$$

with $N_i^0 = S_i^0 + Q_i^0$ and $M^E = (a_{ij}(1-\eta_j^E))_{1\leq i,j\leq n}$. The matrix V_{11} is an irreducible M-matrix with positive column sum. Hence V_{11}^{-1} is non-negative [65]. Moreover, V_{22} and V_{33} are non-negative diagonal matrices, and so are V_{22}^{-1} and V_{33}^{-1}. To go further, the following result on block matrices is instrumental [67].

Lemma 4.5. *Let A be a square nonsingular matrix and R be the block matrix defined by:*

$$R = \begin{pmatrix} A & B \\ C & D \end{pmatrix}$$

where A, B, C and D have the order $k\times k, k\times m, m\times k, m\times m$, respectively. If $D - CA^{-1}B$ is nonsingular, then R is nonsingular and

$$R^{-1} = \begin{pmatrix} A^{-1} + A^{-1}B(D-CA^{-1}B)^{-1}CA^{-1} & -A^{-1}B(D-CA^{-1}B)^{-1} \\ -(D-CA^{-1}B)^{-1}CA^{-1} & (D-CA^{-1}B)^{-1} \end{pmatrix}$$

Lemma 4.5 can be used for the matrix V in (4.17) and (4.18) that has the structure

$$V = \begin{pmatrix} A & B \\ C & D \end{pmatrix}, \text{ where } A = \begin{pmatrix} V_{11} & 0 \\ V_{21} & V_{22} \end{pmatrix}, \ B = \begin{pmatrix} 0 \\ 0 \end{pmatrix}, \ C = \begin{pmatrix} 0 & V_{32} \end{pmatrix}$$
and $D = V_{33}$.

Since A is nonsingular, the matrix V is nonsingular and

$$A^{-1} = \begin{pmatrix} V_{11}^{-1} & 0 \\ -V_{22}^{-1}V_{21}V_{11}^{-1} & V_{22}^{-1} \end{pmatrix}$$
$$\Longrightarrow V^{-1} = \begin{pmatrix} V_{11}^{-1} & 0 & 0 \\ -V_{22}^{-1}V_{21}V_{11}^{-1} & V_{22}^{-1} & 0 \\ V_{33}^{-1}V_{32}V_{22}^{-1}V_{21}V_{11}^{-1} & -V_{33}^{-1}V_{32}V_{22}^{-1} & V_{33}^{-1} \end{pmatrix}.$$

From the expression of the next generation matrix,

$$FV^{-1} = -F_{12}V_{22}^{-1}V_{21}V_{11}^{-1} + F_{13}V_{33}^{-1}V_{32}V_{22}^{-1}V_{21}V_{11}^{-1},$$

it is clear, in light of (4.18), that the first term is due to living infected individuals, while the second term comes from the Ebola-deceased individuals. It is therefore not surprising to have a similar double contribution to the control reproduction number, $\mathcal{R}_c$, obtained, thanks to [66], as the spectral radius of FV^{-1}:

$$\mathcal{R}_c = \rho(FV^{-1}) = \rho(-F_{12}V_{22}^{-1}V_{21}V_{11}^{-1} + F_{13}V_{33}^{-1}V_{32}V_{22}^{-1}V_{21}V_{11}^{-1}). \tag{4.19}$$

The relevance of the control reproduction number is given in the next result [66].

Proposition 4.6. *When $\mathcal{R}_c < 1$, the disease-free equilibrium, $\mathcal{E}_0$, for Model (2.13) is locally asymptotically stable (LAS), and it is unstable when $\mathcal{R}_c > 1$.*

The global asymptotic stability of the disease-free equilibrium is an issue of interest that we address now. This requires some restrictions on the control of the population. First, we assume that all susceptible travelers are negatively screened so that $S_i^0 = N_i^0$, $Q_i^0 = 0$ at the DFE and only latent travelers are quarantined. Mathematically, this means that we introduce from (4.18)

$$\widehat{F} = \begin{pmatrix} 0 & \vdots & \widehat{F}_{12} & \vdots & \widehat{F}_{13} \\ \cdots & & \cdots & & \cdots \\ 0 & \vdots & 0 & \vdots & 0 \\ \cdots & & \cdots & & \cdots \\ 0 & \vdots & 0 & \vdots & 0 \end{pmatrix}, \quad \widehat{V} = \begin{pmatrix} \widehat{V}_{11} & \vdots & 0 & \vdots & 0 \\ \cdots & & \cdots & & \cdots \\ V_{21} & \vdots & V_{22} & \vdots & 0 \\ \cdots & & \cdots & & \cdots \\ 0 & \vdots & V_{32} & \vdots & V_{33} \end{pmatrix}, \tag{4.20}$$

where $\widehat{F}_{12}, \widehat{F}_{13}, \widehat{V}_{11}$ above are defined by:

$$\begin{aligned} &\widehat{F}_{12} = \text{diag}\left(\beta_1, \ldots, \beta_n\right), \ \widehat{F}_{13} = \text{diag}\left(\beta_1 \nu_1, \ldots, \beta_n \nu_n\right), \\ &\widehat{V}_{11} = \text{diag}\left(\sum_{j=2}^n a_{j1}\eta_1^E + \mu_1 + \alpha_1, \ldots, \sum_{j=1}^{n-1} a_{jn}\eta_n^E + \mu_n + \alpha_n\right). \end{aligned} \tag{4.21}$$

We therefore set

$$\mathcal{T} := \rho(\widehat{F}\widehat{V}^{-1}) = \rho(-\widehat{F}_{12}V_{22}^{-1}V_{21}\widehat{V}_{11}^{-1} + \widehat{F}_{13}V_{33}^{-1}V_{32}V_{22}^{-1}V_{21}\widehat{V}_{11}^{-1}),$$

which is obviously given by

$$\mathcal{T} = \max_{1\leq i\leq n}(\mathcal{T}^i) \text{ with } \mathcal{T}^i = \frac{\beta_i \alpha_i (b_i + \nu_i(\mu_i + \delta_i))}{b_i k_i \left((\mu_i + \alpha_i) + \sum_{j=1, j\neq i}^n a_{ji}\eta_i^E\right)}. \tag{4.22}$$

Theorem 4.7. *If $\mathcal{T} < 1$, then the disease-free equilibrium $\mathcal{E}_0$ for Model (2.13) is globally asymptotically stable (GAS) in Γ.*

Proof. Consider on Γ the candidate Lyapunov function

$$\mathcal{L} = \mathcal{L}(S, E, I, D, Q, P, R) = \sum_{i=1}^{n} E_i + \sum_{i=1}^{n} f_i I_i + \sum_{i=1}^{n} g_i D_i,$$

where $f_i, g_i,\ i = 1, \dots, n$ are positive constants to be determined shortly. The derivative along the trajectories, $\dot{\mathcal{L}}$, of $\mathcal{L}$ is

$$\dot{\mathcal{L}} = \sum_{i=1}^{n} \dot{E}_i + \sum_{i=1}^{n} f_i \dot{I}_i + \sum_{i=1}^{n} g_i \dot{D}_i,$$

where the notation $(\dot{S}_i, \dot{E}_i, \dot{I}_i, \dot{D}_i, \dot{Q}_i, \dot{P}_i, \dot{R}_i)$ is used to represent the vector function in the right-hand side of Model (2.13) for the patch number i. Thus,

$$\begin{aligned}
\dot{\mathcal{L}} \le & \sum_{i=1}^{n} (\beta_i (I_i + \nu_i D_i) - (\mu_i + \alpha_i) E_i) - \sum_{i,j=1, j\neq i}^{n} a_{ji} \eta_i^E E_i \\
& + \sum_{i=1}^{n} f_i (\alpha_i E_i - (\mu_i + \delta_i + \gamma_i) I_i) \\
& + \sum_{i=1}^{n} g_i ((\mu_i + \delta_i) I_i - b_i D_i) \\
= & \sum_{i=1}^{n} \left(f_i \alpha_i - (\mu_i + \alpha_i) - \sum_{j=1, j\neq i}^{n} a_{ji} \eta_i^E \right) E_i \\
& + \sum_{i=1}^{n} I_i (\beta_i - f_i (\mu_i + \delta_i + \gamma_i) + g_i (\mu_i + \delta_i)) \\
& + \sum_{i=1}^{n} D_i (\beta_i \nu_i - g_i b_i).
\end{aligned}$$

We choose in the sequel the numbers f_i and g_i such that

$$\begin{cases} \beta_i - f_i (\mu_i + \delta_i + \gamma_i) + g_i (\mu_i + \delta_i) = 0, \\ \beta_i \nu_i - g_i b_i = 0 \end{cases}.$$

That is

$$g_i = \frac{\beta_i \nu_i}{b_i}, \quad f_i = \frac{\beta_i (b_i + \nu_i (\mu_i + \delta_i))}{b_i (\mu_i + \delta_i + \gamma_i)}. \tag{4.23}$$

With these values, we have

$$\begin{aligned}
\dot{\mathcal{L}} \le & \sum_{i=1}^{n} \left(\frac{\beta_i \alpha_i (b_i + \nu_i (\mu_i + \delta_i))}{b_i (\mu_i + \delta_i + \gamma_i)} - (\mu_i + \alpha_i) - \sum_{j=1, j\neq i}^{n} a_{ji} \eta_i^E \right) E_i \\
= & \sum_{i=1}^{n} \left((\mu_i + \alpha_i) + \sum_{j=1, j\neq i}^{n} a_{ji} \eta_i^E \right) (\mathcal{T}^i - 1) E_i \\
< & \ 0 \quad \text{when} \quad \mathcal{T} < 1
\end{aligned}$$

This shows that $\mathcal{L}$ is indeed a strict Lyapunov function for Model (2.13) near the DFE, $\mathcal{E}_0$, and the global asymptotic stability of the DFE follows by LaSalle invariance principle. □

Theorem 4.7 guarantees the elimination of the disease if one reduces and maintains the value of $\mathcal{T}$ below one.

In the case where the exit screening is not misleading to record false-positive and false-negative individuals *i.e* all the susceptible travelers are negatively screened, while all the latent travelers are positively screened, one will get $\mathcal{R}_c = \mathcal{T}$. Indeed, in this case: (a) only the latent individuals will be quarantined, (which, as observed earlier, leads to the simplifications $Q_i^0 = 0$, and $S_i^0 = N_i^0, \forall i$ at the DFE); (b) $\eta_i^E = 1, \forall i$. Hence, $\mathcal{T}$ is the basic reproduction number for the model in this case. The corresponding value of $\mathcal{T}$ being its minimum value, relatively small effort is necessary to overcome the disease if the exit screening is not misleading.

The second restrictive condition on the control for the GAS of the DFE is considered in the next theorem the proof of which is based on the decomposition in [68] and is given in Appendix A.

Theorem 4.8. *Assume that the exit screening is 100% negative in the sense that* $\eta_i^S = 0,\ \eta_i^E = 1, \forall i = 1, \dots, n$, *then the disease-free equilibrium is GAS whenever* $\mathcal{R}_c < 1$.

Note that with the parameters estimated in Table 5, we found $\mathcal{R}_c = 0.7737$ and $\mathcal{T} = 0.7767$ meaning that the EVD will be overcome.

Remark 4.9. The comparison of $\mathcal{T}^i$ with the threshold $\mathcal{P}_i^0$ used in Proposition 4.4 for the existence of boundary equilibria is obvious:

$$\mathcal{T}^i \le \mathcal{P}_i^0, \ \forall i = 1, \dots, n. \tag{4.24}$$

Note that the model does not admit positive frontier equilibria when $\mathcal{P}_i^0 \le 1, \ \forall i = 1, \dots, n$.

The quantity

$$\mathcal{P}_0 = \max_{1 \le i \le n} (\mathcal{P}_i^0)$$

is the basic reproduction number of Model (2.13) when all the patches are isolated (that is when there are no migrations between the patches). Eq. (4.24) combined with Theorems 4.7 or 4.8 highlight that less effort is required to control the disease when the patches are interconnected.

5. Numerical simulations

The complexity of Model (2.13) rules out the possibility of completely solving it by analytical techniques. We have developed two NSFD schemes in Appendix C and have proved mathematically that they are dynamically consistent with respect to some properties of the continuous model. In this section, we illustrate the theory presented there by numerical simulations based on our NSFD schemes. For comparison purposes, we also use the ODE 45 (Runge Kutta of order 4). We work in the setting of three patches in order to be close to the West Africa 2014–2016 EVD outbreak that affected simultaneously three countries: Guinea, Liberia, and Sierra Leone. We use the values of the parameters given in Table 5.

Fig. 3 shows that the ODE 45-based solution curves of Model (2.13) fail to stay in the biologically feasible region Γ, while the NSFD schemes do. More precisely, the NSFD schemes resulting total population of human individuals is below the carrying capacity Λ/μ in 2500 weeks (middle and right pictures), which is not the case for the ODE-45 after 200 weeks (left picture). Note that the fact that the nonstandard approach replicates non negative property of solutions, while classical schemes do not is well documented, see for instance [69,70].

Thereafter, only the NSFD Euler scheme, (C.7), is used in this section to illustrate the features of Model (2.13). The figures for the other NSFD scheme, which besides are similar, are presented in Appendix D.

In Fig. 4, the top row of three figures illustrates the dynamic consistency of the NSFD scheme (C.7) with respect to the GAS of the DFE of Model (2.13), as stated in Theorems 4.7 and C.5, assuming that $\mathcal{T} < 1$. Likewise, the bottom row of the three figures deals with the preservation by the NSFD scheme (C.7) of the GAS of the DFE of Model (2.13) in the case where $\mathcal{R}_c < 1 < \mathcal{T}$ for which we did not obtain theoretical results.

From several initial conditions, we plot the curves of infected individuals in all patches during 400 weeks with the values $\mathcal{R}_c = 0.9864 < 1 < \mathcal{T} = 1.1972$. The figures show that the EVD dies out for either NSFD scheme. This motivates the conjecture: "the DFE is GAS for $\mathcal{R}_c < 1 < \mathcal{T}$".

Proposition 4.4 on the existence of positive boundary equilibria for System (2.13) when the matrix $(a_{ij})_{1 \le i,j \le n}$ is reducible is illustrated on the top row of three plots on Fig. 5, for the NSFD scheme (C.7). The values used are $a_{21} = a_{31} = 0$ and $\mathcal{P}_0^1 > 1$, while both $\mathcal{P}_0^2$ and $\mathcal{P}_0^3$ are less than one. This figure highlights that the disease is eliminated in the patches 2 and 3, but it persists in patch 1. However, the figure does not suggest the LAS of the boundary equilibrium $\mathcal{E}_0^1$ when $\mathcal{P}_0^1 > 1$. Finally, the bottom row of three plots of Fig. 5 suggests the existence of an interior equilibrium point when $\mathcal{R}_c > 1$, a fact that we could not prove theoretically. Both NSFD schemes (C.3) and (C.7) initiated at several points stabilize at a positive value as $t \to \infty$.

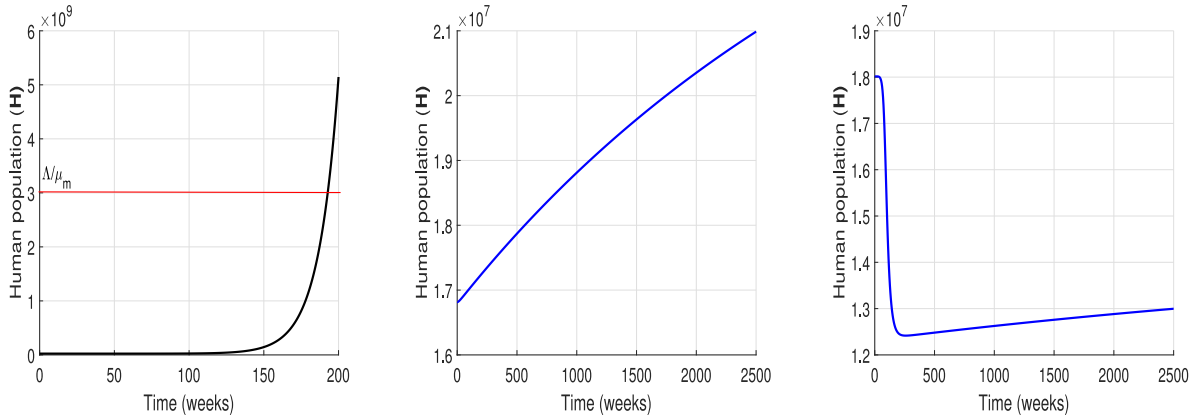

Fig. 3. Dynamic inconsistency of ODE 45 (left picture) and dynamic consistency of NSFD schemes (C.3) & (C.7) (middle and right plots) with respect to remaining in Γ. Figures plotted with the initial conditions $S_1(0) = 4{,}000{,}000, S_2(0) = 4{,}000{,}000$ and $S_3(0) = 4{,}000{,}000$ and the recruitment constant $\Lambda_i = 2000, \forall i = 1, 2, 3, \beta_1 = 0.1017$. The carrying capacity of the total population is $\Lambda/\mu_m = 30{,}000{,}000$. The other parameters and initial conditions are as in Table 5 and Table 4, respectively.

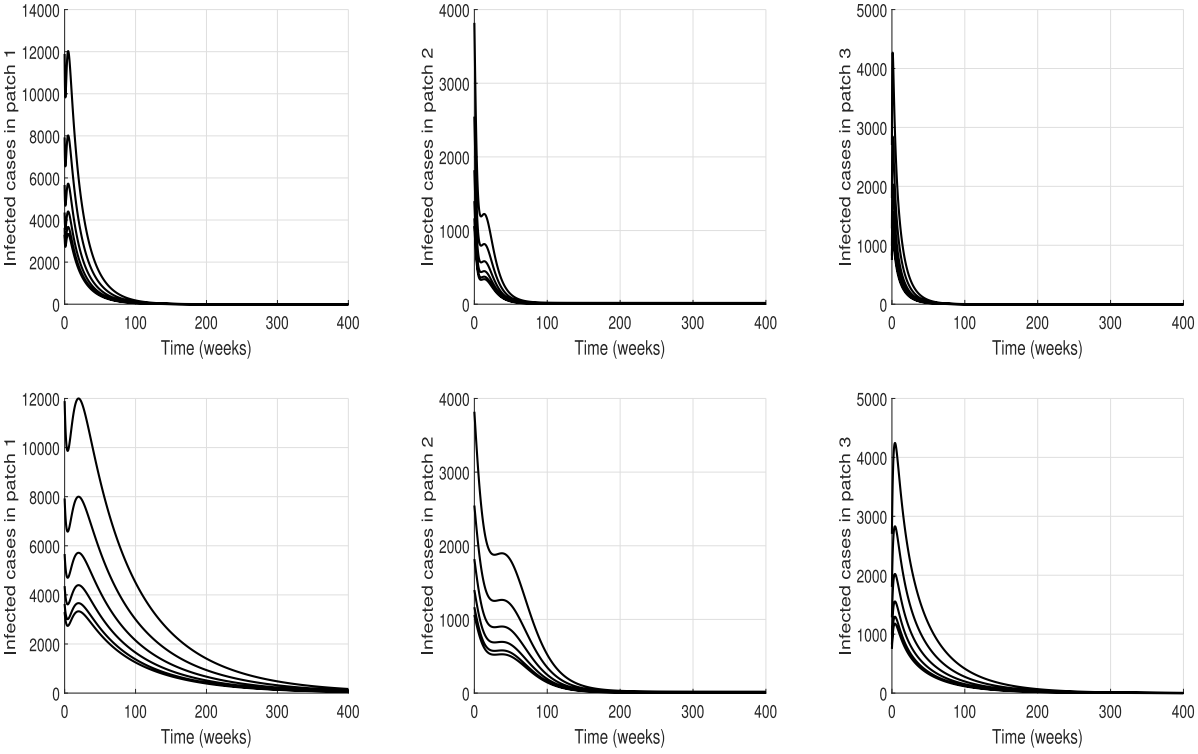

Fig. 4. Graphs of the infected respective compartments I_1, I_2 and I_3 are shown in each row plots for different initial conditions. Top row of 3 plots: Dynamic consistency of NSFD scheme (C.7) with respect to the GAS of Model (2.13), using the parameters in Table 5 and the threshold values $\mathcal{R}_c = 0.7737$ and $\mathcal{T} = 0.7767 < 1$. Bottom row of 3 plots: GAS of the DFE by the NSFD scheme (C.7) when $\mathcal{R}_c < 1 < \mathcal{T}$. Here $\beta_2 = 0.24; \mathcal{R}_c = 0.9864 < 1, \mathcal{T} = 1.1972 > 1$. The other values are as in Table 5.

Given the huge number of parameters involved in our model and seeing that most of these parameters are not available in the literature, we carry out a global sensitivity analysis that is reported in Appendix B. This enables us to numerically assess the influence of the exit screening and the impact of migrations by simulating System (2.13) via the NSFD scheme (C.7) for Guinea, Liberia and Sierra Leone, using the parameters in Table 5. We give, for $i = 1, 2, 3$, three values of η_i^S and η_i^E: (i) $\eta_i^S = \eta_i^E = 0$, (ii) $\eta_i^S = \eta_i^E = 0.3$ and (iii) $\eta_i^S = \eta_i^E = 0.5$. In Fig. 6, the top two rows of three plots each shows that the impact of the exit screening is weak. Apart from the curve of latent individuals in Guinea, all the other curves are merged. The weakness of the exit screening could be attributed to the reduced values of migration rates. This reduction is due to the fact that travel by road (e.g. bus, car, bicycle, foot, etc.), which is the most common means of transport between these neighboring countries was not considered. To account for this means of travel, we assume that the migration rates between these countries are 50 times greater than those estimated in Table 3. Keeping unchanged the other parameters used earlier, we plot in the bottom two rows of Fig. 6 the same curves as before. These rows show that the number of infected in every patches decreases as the exit screening rate increases. This highlights the usefulness of this measure to mitigate the number of EVD-infected individuals.

To overcome the EVD, it is sufficient, in view of Theorem 4.7, to reduce and maintain the explicit threshold, $\mathcal{T}$, below one. It is important to check how this can be achieved through the control of migration and exit screening rates. We address this in the particular case when the migration rates a_{ij} are equal and the exit screening rates η_i^E are equal as well. Fig. 7 shows the bifurcation behavior of the thresholds $\mathcal{T}^i$ in the space (η_i^E, a_{ij}): one sees from these three contour plots that the EVD will be eliminated whenever both parameters η_i^E

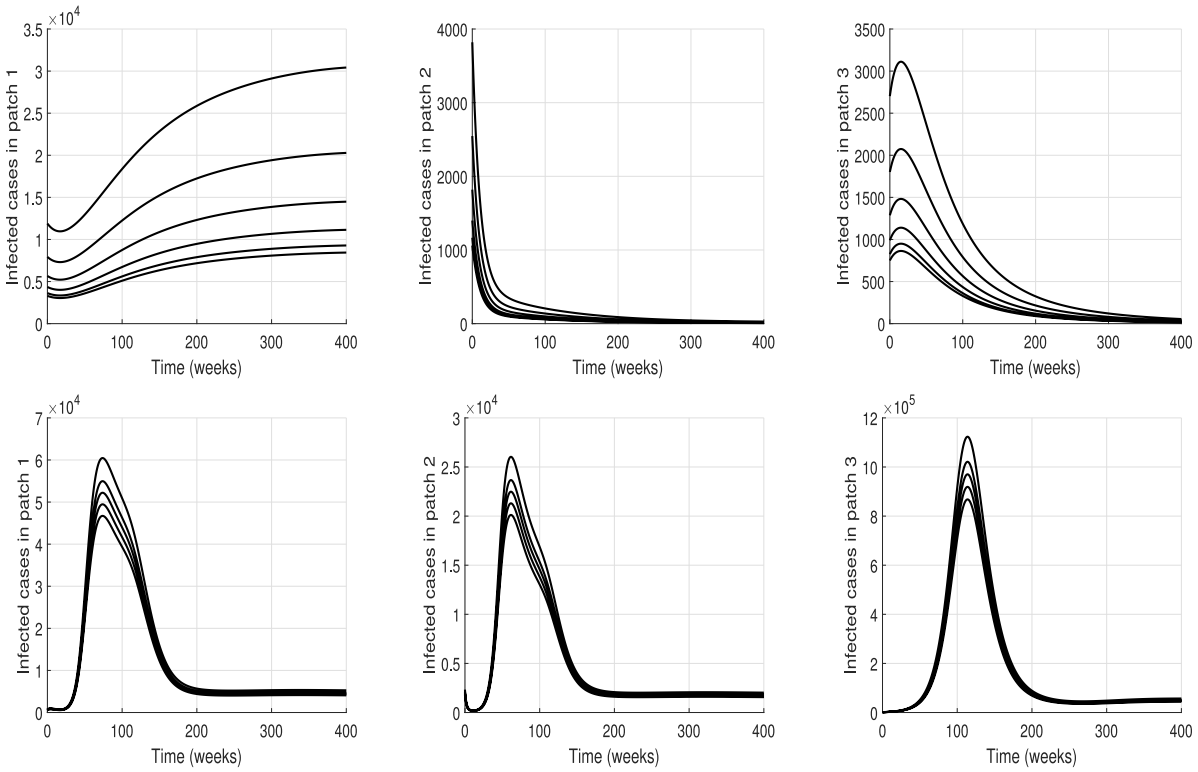

Fig. 5. Graphs of the infected respective compartments I_1, I_2 and I_3 are shown in each row plots for different initial conditions. Top row of three plots: Existence of patch 1 boundary equilibrium and persistence of the disease in patch 1 for $\mathcal{P}_0^1 > 1$ with the NSFD scheme (C.3). We used $\beta_2 = 0.01209, \beta_1 = 0.556, \gamma_2 = 4, \gamma_3 = 0.8$. The other values are in Table 5 and give $\mathcal{P}_0^2 = 0.0099, \mathcal{P}_0^3 = 0.03048, \mathcal{P}_0^1 = 1.6838 > 1, \mathcal{R}_c = 1.6831, \mathcal{T} = 1.6838$. Bottom row of three plots: Existence of a positive interior equilibrium and its stability for the NSFD scheme (C.7) (first row). The values used are in Table E.8 and yield $\mathcal{R}_c = 3.9537 > 1$, $\mathcal{T} = 4.2333 > 1$.

Table 6
Parameters of the model.

Parameters	Epidemiological interpretation	Units
ϑ_i	Recovery rate of infected who belong to the I_i^q compartment.	week^{-1}
θ_i	Recovery rate of individuals who belong to the P_i compartment.	week^{-1}
ϱ_i	Exit rate of the $E_i \& E_i^q$ compartment to the $I_i \& I_i^q$ compartment.	week^{-1}
τ_i^S	Efficiency of entry screening in patch i for individuals in $S_j, S_j^q, j \neq i$.	–
τ_i^Q	Efficiency of entry screening in patch i for individuals in $Q_j, j \neq i$.	–
τ_i^E	Efficiency of entry screening in patch i for individuals in $E_j, E_j^q, j \neq i$.	–
ϖ_i	Mortality rate due to EVD of infected individuals in patch i who belong to the I_i^q compartment.	week^{-1}

and a_{ij} are higher than 0.4. The figure also shows that as the exit screening rates significantly increase, the conditions on high migration rates become more relaxed.

6. Towards a more general metapopulation EVD model

In principle, the content of this section should be part of the Conclusion section, being devoted to our planned future research. However, to avoid having a lengthy conclusion, we opted to include a section here.

From previous sections, it came out clearly that the exit screening, though useful, needs to be combined with other interventions such as the entry screening, especially since many countries implemented the entry screening [71–73]. Below, we highlight the key points of the formulation of a general meta-population model with entry-exit screening intervention.

Obviously, Assumptions A3 in Section 2.1 must be supplemented as follows:

A3* Travelers who test negative for exit screening will undergo entry screening.

For each patch $i = 1, 2, \ldots, n$, the usual compartments S_i, E_i and I_i of susceptible, exposed and infectious individuals are associated with the compartments S_i^q, E_i^q and I_i^q, respectively, defined in Table 6. The superscript "q" on the variables is in accordance with [28,35] to emphasize that among the susceptible individuals who were quarantined, some denoted by S_i^q, came out cleared from the quarantine compartment but cancelled their travel. Typically in [28,35], the susceptible individuals in the S_i^q class return to the initial S_i class from where they progress first to E_i^q if they become exposed to the disease. However, due to the fear created by the Ebola disease, which leads to particular stigmatization of suspected cases [74], individuals in S_i do not practically mix up with those in S_i^q. Hence, the latter individuals follow in our model a parallel progression, leading to a two-group model, contrary to the simplification we considered in Section 2. The force of infection becomes

$$\lambda_i \equiv \lambda_i(t) := \frac{\beta_i(I_i + I_i^q + \nu_i D_i)}{N_i}. \tag{6.1}$$

A description similar to that in Section 2.3 leads to the general entry-exit screening model, where the new parameters are defined in Table 6.

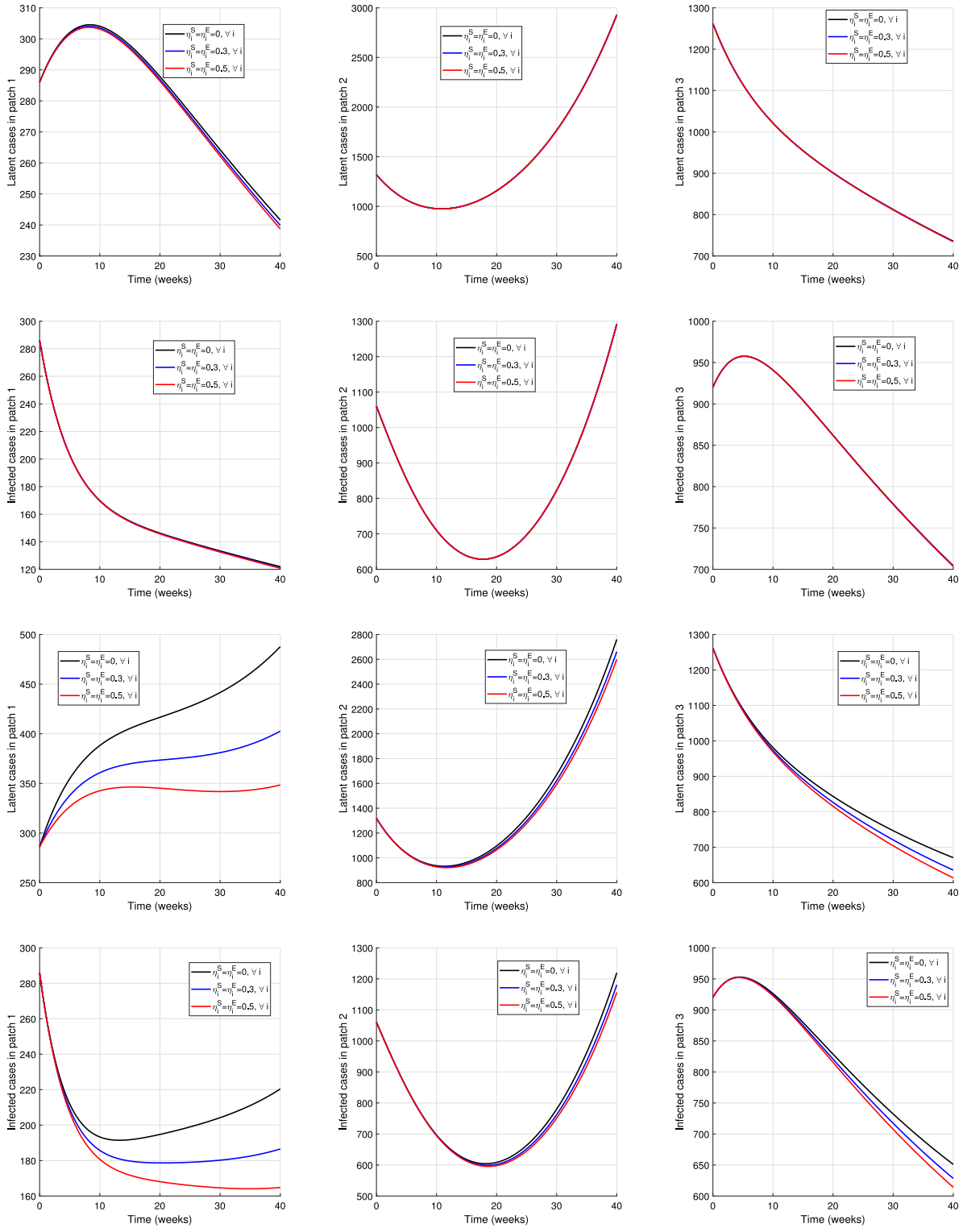

Fig. 6. Top two rows of three plots each: Weak impact of exit screening in the scenarios (i) $\eta_i^S = \eta_i^E = 0$ (dotted curves), (ii) $\eta_i^S = \eta_i^E = 0.3$ (dashed curves), (iii) $\eta_i^S = \eta_i^E = 0.5$ (solid curves), and with migration rates limited to travel by air (see Table 3). We use $\alpha_3 = 0.440$. The other parameters are in Table 5. Bottom two rows of three plots each: Strong impact of exit screening when the migration rates are significantly increased to take into account all types of travels, while keeping unchanged the other parameters.

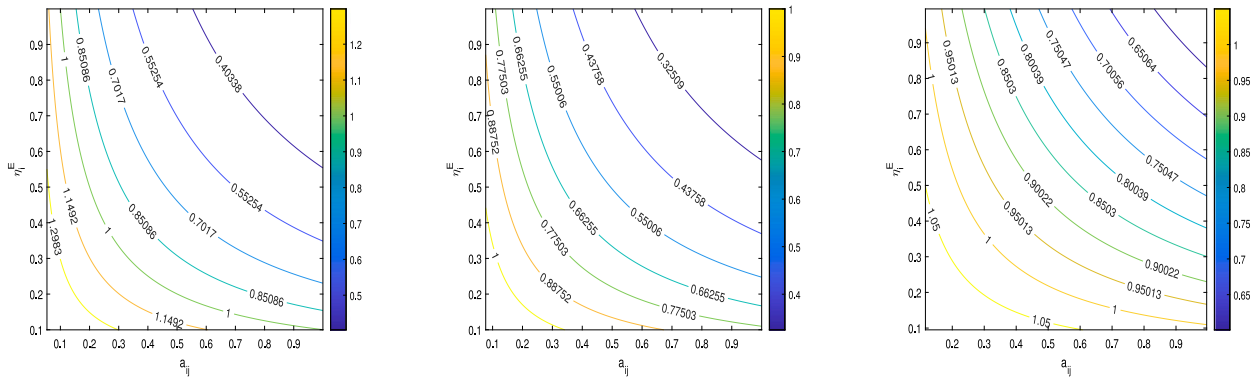

Fig. 7. Contour plot of $\mathcal{T}^i$ versus the migrations and the exit screening rates η_i^E, showing the space zone where the EVD can be eradicated. The first figure is plotted with $b_1 = 0.2$, the second with $b_2 = 0.1$ and the third with $b_3 = 0.2$. The other parameters are on Table 5.

$$
\begin{cases}
\dfrac{dS_i(t)}{dt} &= \Lambda_i - \lambda_i S_i - \mu_i S_i - \displaystyle\sum_{j=1,j\neq i}^{n} a_{ji} S_i + \sum_{j=1,j\neq i}^{n} a_{ij}(1-\eta_j^S)(1-\tau_i^S)S_j,\\
\dfrac{dS_i^q(t)}{dt} &= \displaystyle\sum_{j=1,j\neq i}^{n} (1-\phi)\upsilon_j\xi_{ij}(1-\tau_i^Q)Q_j + (1-\phi)\upsilon_i\xi_{ii}Q_i - \lambda_i S_i^q\\
&\quad -\mu_i S_i^q - \displaystyle\sum_{j=1,j\neq i}^{n} a_{ji} S_i^q + \sum_{j=1,j\neq i}^{n} a_{ij}(1-\eta_j^S)(1-\tau_i^S)S_j^q,\\
\dfrac{dE_i(t)}{dt} &= \lambda_i S_i - \mu_i E_i - \alpha_i E_i - \displaystyle\sum_{j=1,j\neq i}^{n} a_{ji} E_i\\
&\quad + \displaystyle\sum_{j=1,j\neq i}^{n} a_{ij}(1-\eta_j^E)(1-\tau_i^E)E_j,\\
\dfrac{dE_i^q(t)}{dt} &= \lambda_i S_i^q - \mu_i E_i^q - \varrho_i E_i^q - \displaystyle\sum_{j=1,j\neq i}^{n} a_{ji} E_i^q\\
&\quad + \displaystyle\sum_{j=1,j\neq i}^{n} a_{ij}(1-\eta_j^E)(1-\tau_i^E)E_j^q,\\
\dfrac{dI_i(t)}{dt} &= \alpha_i E_i - (\mu_i + \delta_i + \gamma_i)I_i,\\
\dfrac{dI_i^q(t)}{dt} &= \varrho_i E_i^q - (\mu_i + \vartheta_i + \varpi_i)I_i^q,\\
\dfrac{dD_i(t)}{dt} &= (\mu_i + \delta_i)I_i + (\mu_i + \varpi_i)I_i^q - b_i D_i,\\
\dfrac{dQ_i(t)}{dt} &= \displaystyle\sum_{j=1,j\neq i}^{n} a_{ji}\eta_i^E E_i + \sum_{j=1,j\neq i}^{n} a_{ji}\eta_i^S S_i + \sum_{j=1,j\neq i}^{n} a_{ji}\eta_i^S S_i^q\\
&\quad + \displaystyle\sum_{j=1,j\neq i}^{n} a_{ji}\eta_i^E E_i^q\\
&\quad + \displaystyle\sum_{j=1,j\neq i}^{n} a_{ij}(1-\eta_j^E)\tau_i^E E_j + \sum_{j=1,j\neq i}^{n} a_{ij}(1-\eta_j^S)\tau_i^S S_j\\
&\quad + \displaystyle\sum_{j=1,j\neq i}^{n} a_{ij}(1-\eta_j^S)\tau_i^S S_j^q\\
&\quad + \displaystyle\sum_{j=1,j\neq i}^{n} a_{ij}(1-\eta_j^E)\tau_i^E E_j^q + \sum_{j=1,j\neq i}^{n} (1-\phi)\upsilon_j\xi_{ij}\tau_i^Q Q_j\\
&\quad -(\mu_i + \upsilon_i)Q_i,\\
\dfrac{dP_i(t)}{dt} &= \phi\upsilon_i Q_i - (\mu_i + \psi_i + \theta_i)P_i,\\
\dfrac{dR_i(t)}{dt} &= \gamma_i I_i + \theta_i P_i + \vartheta_i I_i^q - \mu_i R_i,
\end{cases}
\tag{6.2}
$$

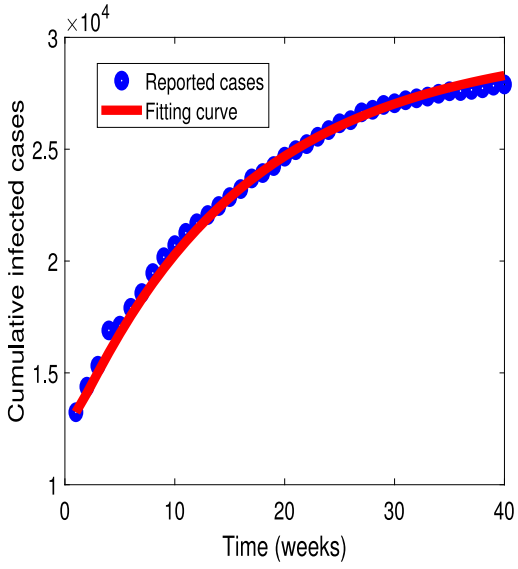

Fig. 8. Curve fitting for Model (6.2) from real data of the 2014–2016 EVD outbreak in Guinea, Liberia, and Sierra Leone [55] from 7 November 2014 to 7 August 2015. The values used for the fitting are in Tables E.8 and 5, respectively.

with $\phi := \phi(S, S^Q, E, E^Q)$, $(S, S^Q, E, E^Q) \in \mathbb{R}^n \times \mathbb{R}^n \times \mathbb{R}^n \times \mathbb{R}^n$ defined as:

$$
\phi(S, S^Q, E, E^Q) = \frac{\sum_{i=1}^{n}(E_i + E_i^Q)}{\sum_{i=1}^{n}(S_i + S_i^Q + E_i + E_i^Q)}. \tag{6.3}
$$

Fig. 8 illustrates the good curve fitting of Model (6.2) to real EVD data, from 07 November 2014 to 07 August 2015 [55], with the initial conditions and parameters values gathered in Appendix E in Tables E.7 and E.8. Considering this good fitting and some preliminary quantitative and qualitative results that we obtained, we are working towards a full mathematical, computational and statistical analysis of the general model (6.2), with the aim to influence policy makers in the fight against EVD.

7. Conclusion

Ebola Virus Disease (EVD) outbreaks in Sub-Saharan Africa often come with unprecedented challenges [24,70]. Of particular interest

to this work is the huge migrations and travels that caused the wide spread of the disease during the 2014–2016 West Africa outbreak. We constructed a metapopulation model to assess the impact, on the transmission dynamics and control of the EVD, of the exit screening at borders that was recommended by WHO for the 2014–2016 West Africa EVD outbreak. Our strategy went beyond this by involving many more interventions such as the quarantine.

Our main findings are summarized as follows:

1. The model was well-fitted and parameterized, using the total reported cases from Guinea, Liberia and Sierra Leone, the countries that were most affected by the 2014–2016 EVD.
2. The control reproduction number, $\mathcal{R}_c$, was computed by the next generation matrix approach, and two additional explicit threshold parameters, $\mathcal{T}$ and $\mathcal{P}_0$, were obtained such that $\mathcal{R}_c \leq \mathcal{T} \leq \mathcal{P}_0$.
3. The unique disease-free equilibrium (DFE) of the model is locally asymptotically stable (LAS) whenever $\mathcal{R}_c < 1$ and unstable if $\mathcal{R}_c > 1$. Moreover, the DFE is globally asymptotically stable (GAS) if $\mathcal{T} < 1$. It is also GAS for $\mathcal{R}_c < 1$ provided that the exit screening is 100% negative.
4. There exists at least one boundary equilibrium if $\mathcal{P}_0 > 1$.
5. The analysis showed the usefulness and benefit of the exit screening measure while suggesting its combination with other measures such as the entry screening for disease control improvement.
6. The recommendations that arise from this work include:
   (a) To train 'legions of disease-fighters' as well as to have the science on the one hand and speak truth to power, and to be connected with the people on the other hand, as promoted by J.J. Muyembe, the first virologist ever to see an Ebola patient and who discovered the Ebola virus in 1976 (see [75]).
   (b) To manage travels and migrations between patches by combining exit screening with other interventions such as entry screening.

Our plan for future research is:

(a) To pursue the analysis of the general metapopulation model with parallel progression subgroups introduced in Section 6.
(b) To develop an optimal control metapopulation model and associated NSFD schemes for a better control of EVD.

CRediT authorship contribution statement

Arsène Jaurès Ouemba Tassé: Writing – review & editing, Writing – original draft, Visualization, Validation, Supervision, Software, Resources, Project administration, Methodology, Investigation, Formal analysis, Data curation, Conceptualization. **Berge Tsanou:** Writing – review & editing, Writing – original draft, Supervision, Resources, Methodology, Investigation, Formal analysis, Conceptualization. **Jean Louis Woukeng:** Supervision, Resources, Project administration, Conceptualization. **Jean M-S Lubuma:** Writing – review & editing, Writing – original draft, Validation, Supervision, Resources, Project administration, Methodology, Investigation, Funding acquisition, Formal analysis, Conceptualization.

Declaration of competing interest

The authors declare no conflict of interest.

Acknowledgments

The authors would like to thank the anonymous reviewers, the Handling Editor and the Editor-in-Chief for suggesting the incorporation of new perspectives that have improved the paper. J.M.-S. Lubuma and A.J. Ouemba Tassé acknowledge the support of the National Research Foundation (NRF), South Africa under the Competitive Program for Rated Researchers (CPRR: Grant no. 138013). They also acknowledge the support of the University of the Witwatersrand, Johannesburg, South Africa under the Science Faculty Start-up Funds for Research and the Postdoctoral Program.

Appendix A. Proof of Theorem 4.8

The proof is based on a decomposition theorem in [68]. Since $\eta_i^E = \eta_i^S = 0, \forall\ i = 1, \dots, n$, the compartments Q_i and P_i simply disappear in Model (2.13). Denote the uninfected compartment and infected compartment by $X = (S, R)$ and $Z = (E, I, D)$, respectively. Using the same notation as in [68], System (2.13) can be rewritten as

$$\begin{cases} \dfrac{dX}{dt} = H(X, Z), \\ \dfrac{dZ}{dt} = G(X, Z),\ G(X, 0) = 0. \end{cases} \tag{A.1}$$

To prove the global asymptotic stability of the DFE for $\mathcal{R}_c < 1$, all we have to do is to show that

- $\mathcal{E}_0 := S^0$ is GAS for the sub-system

$$\begin{aligned} \frac{dX}{dt} = H(X, 0) := [&\Lambda_1 - \mu_1 S_1 - \sum_{j=1, j\neq 1}^{n} a_{j1} S_1 + \sum_{j=1, j\neq 1}^{n} a_{1j} S_j, \cdots, \Lambda_n - \mu_n S_n \\ &- \sum_{j=1, j\neq n}^{n} a_{jn} S_n \\ &+ \sum_{j=1, j\neq n}^{n} a_{nj} S_j, 0 \cdots 0]^T \end{aligned} \tag{A.2}$$

- $G(X, Z) = LZ - \widehat{G}(X, Z)$ where $\widehat{G}(X, Z) \geq 0$ in Γ and $L = D_Z G(S^0, 0, 0, 0, 0)$, the Jacobian matrix of G evaluated at the disease-free equilibrium, is a Metzler matrix.

Using the analog of the vector notation S and Λ in (2.3), the GAS of $\mathcal{E}_0$ for the system (A.2) is equivalent to the GAS of S^0 for the system

$$\frac{dS}{dt} = \Lambda - \widetilde{C} S, \tag{A.3}$$

where $\widetilde{C}$ is the following nonsingular M-matrix with all the eigenvalues of $-C$ having negative real parts:

$$\widetilde{C} = \begin{pmatrix} \mu_1 + \sum_{j=1, j\neq 1}^{n} a_{j1} & -a_{12} & \cdots & -a_{1n} \\ -a_{21} & \mu_2 + \sum_{j=1, j\neq 2}^{n} a_{j2} & \cdots & -a_{2n} \\ \vdots & \vdots & \vdots & \vdots \\ -a_{n1} & -a_{n2} & \cdots & \mu_n + \sum_{j=1, j\neq n}^{n} a_{jn} \end{pmatrix}. \tag{A.4}$$

It follows then from [65] that the solution $S(t) = -e^{-t\widetilde{C}} \widetilde{C}^{-1} \Lambda + \widetilde{C}^{-1} \Lambda$ of (A.3) converges to $\widetilde{C}^{-1} \Lambda$. This proves the claim in the above first bullet. Regarding the claim in the second bullet, one can, in the above decomposition of G, like in [68], write the matrix L in terms of the matrices F and V in (4.17) and specify L (see the equation in Box II).

It is clear that L is indeed a Metzler matrix, and its eigenvalues have real parts less than zero whenever $\mathcal{R}_c < 1$. We then take

$$\widehat{G}(X, Y) := \left(\beta_1 (I_1 + \nu_1 D_1) \left(1 - \frac{S_1}{N_1}\right), \cdots, \beta_n (I_n + \nu_n D_n) \left(1 - \frac{S_n}{N_n}\right), \right.$$

$$
\begin{aligned}
L &= F - V \\
&= \begin{pmatrix}
-(\mu_1+\alpha_1) - \sum_{j=1,j\neq 1}^{n} a_{j1} & \cdots & a_{1n} & \beta_1 & \cdots & 0 & \beta_1\nu_1 & \cdots & 0 \\
\vdots & \vdots & \vdots & \vdots & \vdots & \vdots & \vdots & \vdots & \\
a_{n1} & \cdots & -(\mu_n+\alpha_n) - \sum_{j=1,j\neq n}^{n} a_{jn} & 0 & \cdots & \beta_n & 0 & \cdots & \beta_n\nu_n \\
\alpha_1 & \cdots & 0 & -k_1 & \cdots & 0 & 0 & \ldots & 0 \\
\vdots & \vdots & \vdots & \vdots & \vdots & \vdots & \vdots & \vdots & \\
0 & \ldots & \alpha_n & 0 & \ldots & -k_n & 0 & \ldots & 0 \\
0 & \ldots & 0 & (\mu_1+\delta_1) & \ldots & 0 & -b_1 & \ldots & 0 \\
\vdots & \vdots & \vdots & \vdots & \vdots & \vdots & \vdots & \vdots & \\
0 & \ldots & 0 & 0 & \ldots & (\mu_n+\delta_n) & 0 & \ldots & -b_n
\end{pmatrix}.
\end{aligned}
$$

Box II.

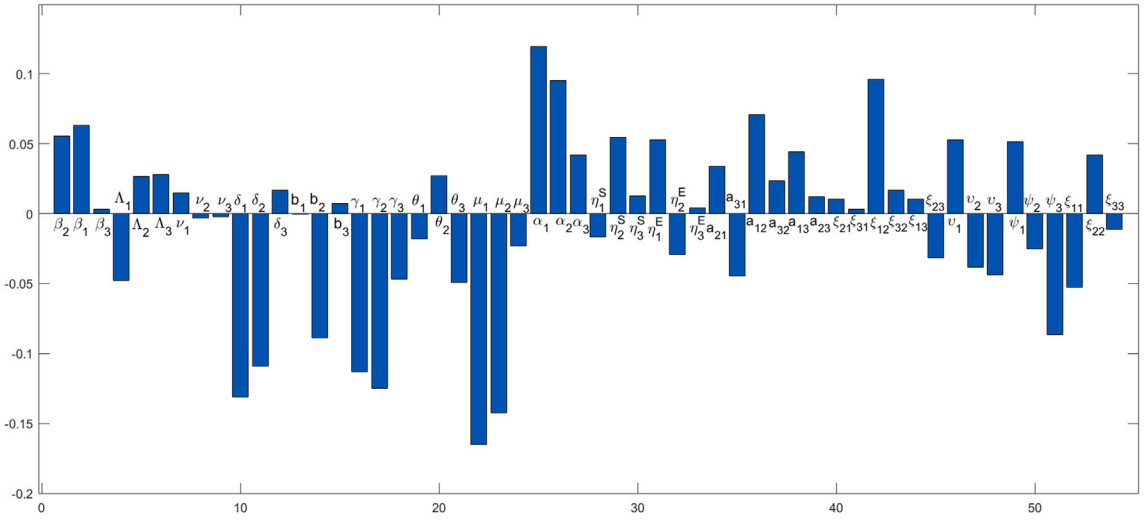

Fig. B.9. PRCCs of $I_1 + I_2 + I_3$.

$$
\left(0, \cdots, 0, \ldots, 0\right)^T \geq 0.
$$

Hence, the global asymptotic stability of the DFE follows when $\mathcal{R}_c < 1$. □

Appendix B. Global sensitivity analysis

We carry out a global sensitivity analysis of $(I_1 + I_2 + I_3)$, using the Latin Hypercube Sampling (LHS) scheme on the understanding that values outside the interval $(-0.05, 0.05)$ are considered to have a significant impact. The results used in Section 5 and presented on Fig. B.9 show that the parameters α_1 & α_2 of the transitions from E_1 & E_2 compartments to I_1&I_2 compartments are the more influential ones with regard to the increase of the infective individuals. The same thing applies to the parameters $\mu_1, \mu_2, \delta_1, \gamma_2$ and γ_1 with regard to the decrease in the total number of infected individuals. Moreover, the parameters $(\eta_2^S, \eta_3^S, \eta_1^E, \eta_3^E)$ and (η_1^S, η_2^E) influence the increase and the decrease of infected individuals, respectively.

Appendix C. Nonstandard finite difference schemes

We construct in this section two nonstandard finite difference (NSFD) schemes that are dynamically consistent with respect to Model (2.13). We follow Mickens' rules presented in [25,76] and formalized in [69]. Let

$$
\mathcal{X}^k = (S^k, E^k, I^k, D^k, Q^k, P^k, R^k)^T
$$

denote an approximation of the solution $\mathcal{X}(t_k)$ at $t = t_k$, where $t_k = k\Delta t$, $k \in \mathbb{N}$ and $h = \Delta t > 0$ is the step size.

We start with the NSFD backward–forward Euler scheme based on the destructive-productive structure of Model (2.13) [77] and the Gauss–Seidel cycle as done in [78]. Considering a nontrivial denominator function, r, defined by

$$
r \equiv r(h) = \frac{1 - e^{-qh}}{q} = h + \mathcal{O}(h^2), \tag{C.1}
$$

where

$$
(1 - r \sum_{j=1,j\neq i}^{n} a_{ji}) \geq 0, \ (1 - r\upsilon_i) \geq 0, \ \forall\, i.
$$

and, with $\upsilon_M = \max_{1\le i\le n}(\upsilon_i)$,

$$q \ge \min(\frac{1}{\upsilon_M}, \sum_{i,j=1,i\neq j}^{n} a_{ji}), \tag{C.2}$$

the NSFD backward–forward scheme, reads as follows for $i = 1, 2, \dots, n$:

$$\begin{cases}
\frac{S_i^{k+1}-S_i^k}{r} &= \Lambda_i - \lambda_i^k S_i^{k+1} - \mu_i S_i^{k+1} - \sum_{j=1,j\neq i}^{n} a_{ji} S_i^k \\
&\quad + \sum_{j=1,j\neq i}^{n} a_{ij}(1-\eta_j^S) S_j^k \\
&\quad + \sum_{j=1}^{n} (1-\phi_j(S_j^k, E_j^k))\upsilon_j \xi_{ij} Q_j^k, \\
\frac{E_i^{k+1}-E_i^k}{r} &= \lambda_i^k S_i^{k+1} - \mu_i E_i^{k+1} - \alpha_i E_i^{k+1} - \sum_{j=1,j\neq i}^{n} a_{ji} E_i^k \\
&\quad + \sum_{j=1,j\neq i}^{n} a_{ij}(1-\eta_j^E) E_j^k, \\
\frac{I_i^{k+1}-I_i^k}{r} &= \alpha_i E_i^{k+1} - (\mu_i + \delta_i + \gamma_i) I_i^{k+1}, \\
\frac{D_i^{k+1}-D_i^k}{r} &= (\mu_i + \delta_i) I_i^{k+1} - b_i D_i^{k+1}, \\
\frac{Q_i^{k+1}-Q_i^k}{r} &= \sum_{j=1,j\neq i}^{n} a_{ji}\eta_i^E E_i^k + \sum_{j=1,j\neq i}^{n} a_{ji}\eta_i^S S_i^k - \mu_i Q_i^{k+1} - \upsilon_i Q_i^k, \\
\frac{P_i^{k+1}-P_i^k}{r} &= \phi_i(S_i^k, E_i^k)\upsilon_i Q_i^k - (\mu_i + \psi_i + \theta_i) P_i^{k+1}, \\
\frac{R_i^{k+1}-R_i^k}{r} &= \gamma_i I_i^{k+1} + \theta_i P_i^{k+1} - \mu_i R_i^{k+1}.
\end{cases} \tag{C.3}$$

We derive the following result:

Theorem C.1. *The NSFD scheme (C.3) is dynamically consistent with the continuous Model (2.13) in the sense that it is a discrete dynamical system on the biologically feasible region Γ of the continuous System (2.13) and it enjoys the discrete conservation law (C.4) below.*

Proof. By construction, the non negativity of solutions is preserved. The forward invariance of Γ follows from the discrete conservation laws,

$$\begin{aligned}
\frac{\mathbf{H}^{k+1}-\mathbf{H}^k}{r} &= \sum_{i=1}^{n} [\Lambda_i - \mu_i(S_i^{k+1} + E_i^{k+1} + I_i^{k+1} + Q_i^{k+1} + P_i^{k+1} + R_i^{k+1}) \\
&\quad - b_i D_i^{k+1} - \psi_i P_i^{k+1}]. \\
\frac{\mathbf{D}^{k+1}-\mathbf{D}^k}{r} &= \sum_{i=1}^{n} [(\mu_i + \delta_i) I_i^{k+1} - b_i D_i^{k+1}],
\end{aligned} \tag{C.4}$$

obtained by simple computation and to which the discrete Gronwall inequality is applied. □

Unlike the NSFD scheme (C.3) where both Mickens' rules on the nontrivial denominator function of discrete derivatives (i.e. Rule 2) and the nonlocal discretization of nonlinear terms (i.e. Rule 3) [76] were used, the second NSFD scheme, the NSFD forward Euler scheme, we proposed is only based on Rule 2 in which the denominator function is r in (C.3). The parameter q is such that

$$q \ge \min(\frac{1}{a^M}, \frac{1}{\alpha^M}, \frac{1}{\gamma^M}, \frac{1}{b^M}, \frac{1}{\upsilon^M}, \frac{1}{\theta^M}, \frac{1}{\mu^M}). \tag{C.5}$$

and

$$q > \frac{|\vartheta|^2}{2|\Re e\vartheta|}, \tag{C.6}$$

where ϑ is any eigenvalue of the Jacobian matrix of the continuous Model (2.13) at the DFE. The NSFD forward Euler schemes reads as follows:

$$\begin{cases}
\frac{S_i^{k+1}-S_i^k}{r} &= \Lambda_i - \lambda_i^k S_i^k - \mu_i S_i^k - \sum_{j=1,j\neq i}^{n} a_{ji} S_i^k + \sum_{j=1,j\neq i}^{n} a_{ij}(1-\eta_j^S) S_j^k \\
&\quad + \sum_{j=1}^{n} (1-\phi_j(S_j^k, E_j^k))\upsilon_j \xi_{ij} Q_j^k, \\
\frac{E_i^{k+1}-E_i^k}{r} &= \lambda_i^k S_i^k - \mu_i E_i^k - \alpha_i E_i^k - \sum_{j=1,j\neq i}^{n} a_{ji} E_i^k \\
&\quad + \sum_{j=1,j\neq i}^{n} a_{ij}(1-\eta_j^E) E_j^k, \\
\frac{I_i^{k+1}-I_i^k}{r} &= \alpha_i E_i^k - (\mu_i + \delta_i + \gamma_i) I_i^k, \\
\frac{D_i^{k+1}-D_i^k}{r} &= (\mu_i + \delta_i) I_i^k - b_i D_i^k, \\
\frac{Q_i^{k+1}-Q_i^k}{r} &= \sum_{j=1,j\neq i}^{n} a_{ji}\eta_i^E E_i^k + \sum_{j=1,j\neq i}^{n} a_{ji}\eta_i^S S_i^k - \mu_i Q_i^k - \upsilon_i Q_i^k, \\
\frac{P_i^{k+1}-P_i^k}{r} &= \phi_i(S_i^k, E_i^k)\upsilon_i Q_i^k - (\mu_i + \psi_i + \theta_i) P_i^k, \\
\frac{R_i^{k+1}-R_i^k}{r} &= \gamma_i I_i^k + \theta_i P_i^k - \mu_i R_i^k.
\end{cases} \tag{C.7}$$

A similar result to Theorem C.1 is stated below.

Theorem C.2. *The NSFD forward Euler scheme (C.7) is a discrete dynamical system on the biologically feasible region, Γ, of the continuous Model (2.13).*

When $\mathcal{R}_c < 1$, the NSFD forward Euler scheme is elementary stable [69,76], a fact that can be deduced from the next theorem.

Theorem C.3. *Under the conditions (C.5) and (C.6), the disease-free fixed (DFF) point of the NSFD scheme (C.7) is exactly the disease-free equilibrium of the continuous model and it preserves its stability. That is the DFF is LAS if $\mathcal{R}_c < 1$, and unstable if $\mathcal{R}_c > 1$.*

The decomposition theorem in [68] that is abundantly used to prove the GAS of the DFE was recently extended to discrete dynamical systems in [24, Theorem 5.3]. Combining this discrete analog theorem with the earlier proof of the stability of the DFE for $\mathcal{R}_c < 1$ and using (C.6), we readily obtain the following global stability result:

Theorem C.4. *Assume that the exit screening is 100% negative in the sense that $\eta_i^S = \eta_i^E = 0, \forall\, i = 1, \dots, n$. Then, Model (C.7) is dynamically consistent with the GAS of the DFE of the continuous model when $\mathcal{R}_c < 1$.*

A more general result on the dynamic consistency of the NSFD scheme (C.7) with respect to the global asymptotic stability of the DFE is provided in the next theorem.

Theorem C.5. *When $\mathcal{T} < 1$, the DFF for the discrete System (C.7) is GAS.*

Proof. This theorem follows from LaSalle invariance principle, using the following discrete Lyapunov function:

$$\mathcal{L}^k = \frac{1}{r}(\sum_{i=1}^{n} E_i^k + \sum_{i=1}^{n} f_i I_i^k + \sum_{i=1}^{n} g_i D_i^k),$$

where f_i and g_i are defined in (4.23). □

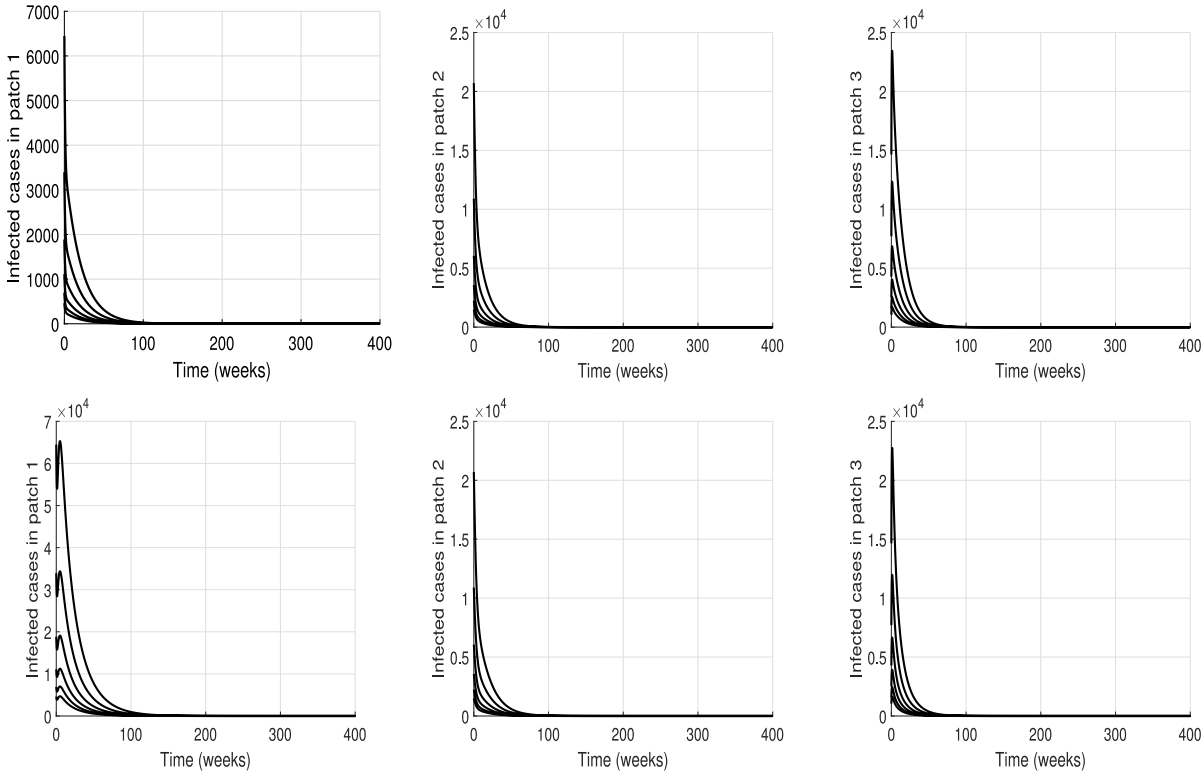

Fig. D.10. Graphs of the infected respective compartments I_1, I_2 and I_3 are shown in each row plots for different initial conditions. *Top row of 3 plots:* Dynamic consistency of NSFD scheme (C.3) with respect to the GAS of Model (2.13), using the parameters in Table 5 and the threshold values $\mathcal{R}_c = 0.7737$ and $\mathcal{T} = 0.7767 < 1$. *Bottom row of 3 plots:* GAS of the DFE by the NSFD scheme (C.3) when $\mathcal{R}_c < 1 < \mathcal{T}$. Here $\beta_2 = 0.24; \mathcal{R}_c = 0.9864 < 1, \mathcal{T} = 1.1972 > 1$. The other values are as in Table 5.

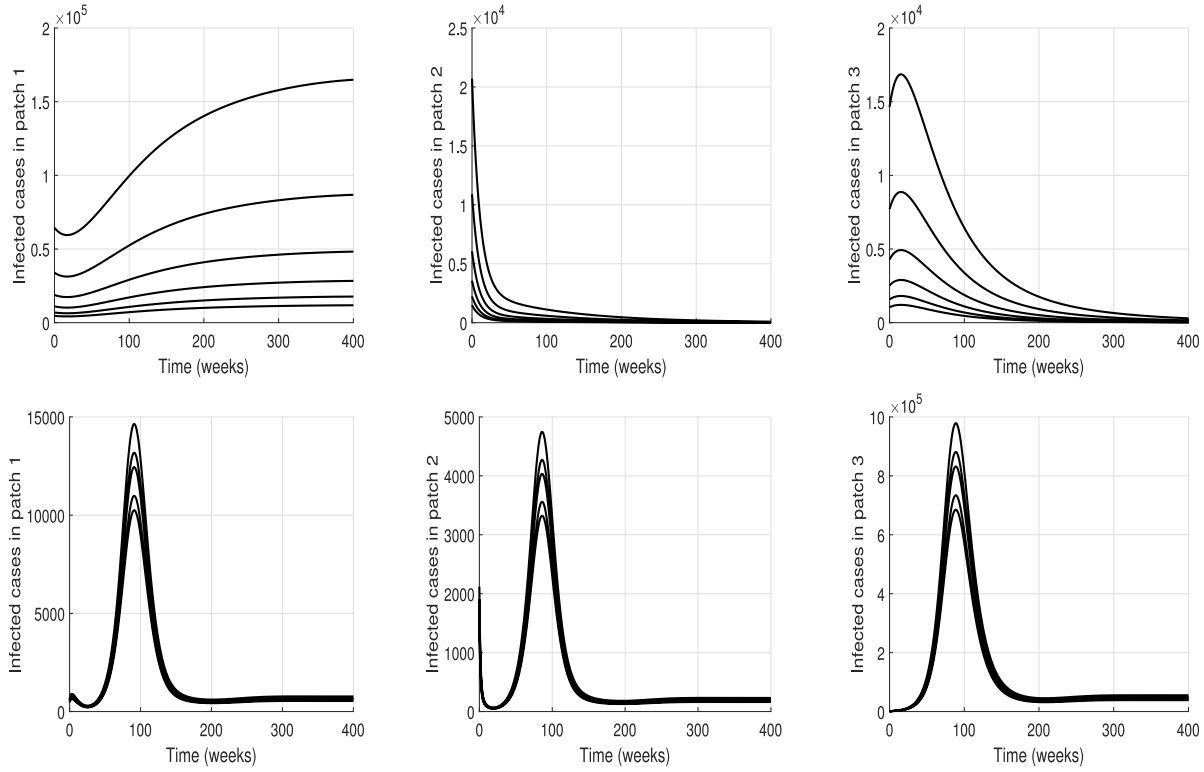

Fig. D.11. Graphs of the infected respective compartments I_1, I_2 and I_3 are shown in each row plots for different initial conditions. *Top row of three plots:* Existence of patch 1 boundary equilibrium and persistence of the disease in patch 1 for $\mathcal{P}_0^1 > 1$ with the NSFD scheme (C.3). We used $\beta_2 = 0.01209, \beta_1 = 0.556, \gamma_2 = 4, \gamma_3 = 0.8$. The other values are in Table 5 and give $\mathcal{P}_0^2 = 0.0099, \mathcal{P}_0^3 = 0.03048, \mathcal{P}_0^1 = 1.6838 > 1, \mathcal{R}_c = 1.6831, \mathcal{T} = 1.6838$. *Bottom row of three plots:* Existence of a positive interior equilibrium and its stability for the NSFD scheme (C.3). The values used are in Table E.8 and yield $\mathcal{R}_c = 3.9537 > 1$, $\mathcal{T} = 4.2333 > 1$.

Table E.7
Initial values of the variables for Model (6.2).

Countries	E(0)	I(0)	D(0)	Q(0)	P(0)	R(0)	$S^q(0)$	$E^q(0)$	$I^q(0)$	Total
Guinea	280	236	286	186	286	286	100	50	50	1760
Liberia	1119	860	1060	760	1060	1060	300	200	200	6619
Sierra Leone	1062	620	720	520	720	720	200	200	100	4862

Table E.8
Parameters values to calibrate System (6.2) and parameters used to plot the Fig. 5.

Par.	Est. Val.	Source	Val. Fig. 5	Par.	Est. Val.	Source	Val. Fig. 5
η_1^E	0.9671	Fitted	0.5433	τ_1^S	0.327	Fitted	
μ_1	0.0002	[58]	0.00004	υ_1	0.4844	Fitted	0.51868
β_1	0.2018	Fitted	0.0015	β_2	0.1077	Fitted	0.0006312
β_3	0.2492	Fitted	0.3128	υ_2	0.2131	Fitted	0.53906
ν_1	1.3672	Fitted	0.508	ν_2	1.3071	Fitted	3.0656
ν_3	0.4718	Fitted	0.867	τ_3^E	0.9930	Fitted	0.022
δ_1	0.857	[59]	0.857	δ_2	0.75	[60]	0.075
δ_3	0.5	[50]	0.5	υ_3	0.4518	Fitted	0.5764
ψ_1	0.3	[41]	0.3	ψ_2	0.4	[39]	0.04
ψ_3	0.5	[50]	0.5	ξ_{21}	0.1109	Fitted	0.0764
ξ_{31}	0.1735	Fitted	0.4679	ξ_{12}	0.0072	Fitted	0.5018
ξ_{11}	0.7325	Fitted	0.4557	ξ_{22}	0.1356	Fitted	0.5109
ξ_{33}	0.2922	Fitted	0.7053	τ_2^S	0.0791	Fitted	
ξ_{32}	0.7506	Fitted	0.4873	ξ_{13}	0.0851	Fitted	0.2328
ξ_{23}	0.136	Fitted	0.0612	a_{21}	0.000064	Estimated	0.000284
a_{31}	0.0001	Estimated	0.0121	a_{12}	0.00054	Estimated	0.05548
a_{32}	0.0001	Estimated	0.0150	a_{13}	0.00063	Estimated	0.000122
a_{23}	0.000036	Estimated	0.0131	b_3	0.5	[50]	0.5
b_1	1/2.01	[50]	1/2.01	b_2	1/4.5	[60]	1/4.5
γ_1	0.0059	[51]	0.059	γ_2	0.026767	[51]	0.6026767
θ_1	0.001120	[51]	0.75	θ_2	0.031486	[51]	0.075
θ_3	0.015743	[51]	0.75	γ_3	0.010038	[51]	0.010038
τ_3^S	0.3107	Fitted		μ_2	0.0002	[58]	14/1000
μ_3	0.0002	[58]	10.17/1000	π_i, $\forall\, i$	0.03703	[61]	0.03703
α_1	7.6999	Fitted	10.5239	α_2	3.8393	Fitted	0.083333
α_3	0.7607	Fitted	0.1	η_1^S	0.2019	Fitted	0.21
η_2^S	0.1978	Fitted	0.21	η_3^S	0.1514	Fitted	0.2317
η_2^E	0.5539	Fitted	0.2226	η_3^E	0.4008	Fitted	0.4229
τ_1^Q	0.2067	Fitted		τ_2^Q	0.4515	Fitted	
τ_3^Q	0.2013	Fitted		ϱ_1	0.4355	Fitted	
ϱ_2	2.1073	Fitted		ϱ_3	0.2717	Fitted	
ϑ_1	0.3906	Fitted		ϑ_2	0.0725	Fitted	
ϑ_3	0.9384	Fitted		ϖ_1	0.3668	Fitted	
ϖ_2	0.4316	Fitted		ϖ_3	0.3509	Fitted	
τ_1^E	0.1536	Fitted		τ_2^E	0.709	Fitted	

Appendix D. Model simulations using the scheme (C.7)

In Fig. D.10, the top row of three figures illustrates the dynamic consistency of the NSFD scheme (C.3) with respect to the GAS of the DFE of Model (2.13), as stated in Theorems 4.7 and C.5, assuming that $\mathcal{T} < 1$. Likewise, the bottom row of the three figures deals with the preservation by the NSFD scheme (C.3) of the GAS of the DFE of Model (2.13) in the case where $\mathcal{R}_c < 1 < \mathcal{T}$ for which we did not obtain theoretical results.

Proposition 4.4 on the existence of positive boundary equilibria for System (2.13) when the matrix $(a_{ij})_{1\leq i,j\leq n}$ is reducible is illustrated on the top row of three plots on Fig. D.11, for the NSFD scheme (C.3), respectively. The values used are $a_{21} = a_{31} = 0$ and $\mathcal{P}_0^1 > 1$, while both $\mathcal{P}_0^2$ and $\mathcal{P}_0^3$ are less than one. This figure highlights that the disease is eliminated in the patches 2 and 3, but it persists in patch 1. However, the figure does not suggest the LAS of the boundary equilibrium $\mathcal{E}_0^1$ when $\mathcal{P}_0^1 > 1$. Finally, the bottom row of three plots of Fig. D.11 suggest the existence of an interior equilibrium point when $\mathcal{R}_c > 1$.

Appendix E. Initial conditions and estimated values for model (6.2)

See Tables E.7 and E.8.

Data availability

Data will be made available on request.

References

[1] WHO, Ebola Virus Disease fact sheet (103) (Fact sheet), 2023, (Facts). (Accessed 06 July 2023).

[2] CDC, Ebola disease distribution map: Cases of Ebola virus disease in Africa since 1976, 2023, (Map). (Accessed 15 February 2024).

[3] E.I. Ohimain, D. Silas-Olu, 2013–2016 Ebola virus disease outbreak in West Africa, Curr. Opin. Pharmacol. 60 (2021) 360–365.

[4] OAG, Ebola Statistics: For the most up-to-date information regarding the Ebola crisis please see our commentary below, 2014, (Ebola Statistics). (Accessed 03 May 2023).

[5] UNICEF Guinea, Migration profiles, 2014, (Guinea). (Accessed 26 April 2023).

[6] UNICEF Liberia, Migration profiles, 2014, (Liberia). (Accessed 26 April 2023).

[7] UNICEF Sierra Leone, Migration profiles, 2014, (Sierra Leone). (Accessed 26 April 2023).

[8] C.L. Althaus, N. Low, E.O. Musa, F. Schuai, S. Gsteiger, Ebola virus disease outbreak in Nigeria: Transmission dynamics and rapid control, Epidemics 11 (2015) 80–84.

[9] D. Salem, R. Smith, A Mathematical Model of Ebola Virus Disease: Using Sensitivity Analysis to Determine Effective Intervention Targets, SCS, 2016, pp. 16–23, (EVD model).

[10] C.M. Brown, A.E. Aranas, G.A. Benenson, G. Brunette, M. Cetron, T.-H. Chen, et al., Airport exit and entry screening for Ebola-August-November 10, Medscape 63 (49) (2014) 1163–1167.

[11] WHO, Implementing exit screening at airport of a country with initial cases of Ebola virus disease transmission, 2014, pp. 1–5, (Implementing Exit Screening at Airport).

[12] WHO, Interim guidance for Ebola virus disase: Exit screening at airports, ports and land crossings, 2014, pp. 1–25, (WHO screening guidance).

[13] S. Kim, A.C. Tridane Chang, Human migration and mosquito-borne diseases in Africa, Math. Popul. Stud. 23 (2016) 123–146.

[14] BBC, Is it worth screening for Ebola at airports? 2014, (Screening at Airports). (Accessed 23 April 2024).

[15] O. Zakary, M. Rachik, I. Elmouki, A multi-regional epidemic model for controlling the spread of Ebola: Awareness, treatment, and travel-blocking optimal control approaches, Math. Methods Appl. Sci. 40 (2017) 1265–1279.

[16] W.O. Kermack, A.G.A. McKendrick, Contribution to the mathematical theory of epidemics, Proc. R. Soc. Lond. A 115 (1927) 700–721.

[17] I. Area, F. Ndaïrou, J.J. Nieto, C.J. Silva, D.F.M. Torres, Ebola model and optimal control with vaccination constraints, J. Ind. Manag. Optim. 278 (2017) 1–21.

[18] T. Berge, A.J. Ouemba Tassé, H.M. Tenkam, J. Lubuma, Mathematical modeling of contact tracing as a control strategy of Ebola virus disease, Int. J. Biomath. 11 (2018) 1850093–1–36.

[19] G. Ngwa, M.I. Teboh-Ewungkem, A mathematical model with quarantine states for the dynamics of Ebola virus disease in human populations, Comput. Math. Methods Med. 2016 (2016) 1–29.

[20] B. Tsanou, S. Bowong, J. Mbang, J. Lubuma, Assessing the impact of the environmental contamination on the transmission of Ebola Virus Disease (EVD), J. Appl. Math. Comput. 55 (2017) 205–243.

[21] B. Espinoza, V. Moreno, D. Bichara, C. Castillo-Chavez, Assessing the efficiency of movement restriction as a control strategy of Ebola, in: Mathematical and Statistical Modeling for Emerging and Re-Emerging Infectious Diseases, 2016, pp. 123–145, (Movement restrictions.

[22] B. Ivorra, D. Ngom, A.M. Ramos, Be-CoDis: A mathematical model to predict the risk of human diseases spread between countries-validation and application to the 2014–2015 Ebola virus disease epidemic, Bull. Math. Biol. 77 (2015) 1668–1704.

[23] X. Wang, S. Liu, L. Wang, W. Zhang, An epidemic patchy model with entry-exit screening, Bull. Math. Biol. 77 (2015) 1237–1255.

[24] M. Chapwanya, J.M.-S. Lubuma, Y. Terefe, B. Tsanou, Analysis of war and conflict effect on the transmission dynamics of the tenth Ebola outbreak in the Democratic Republic of Congo, Bull. Math. Biol. 84 (2002) 136, 1–48.

[25] R.E. Mickens, Nonstandard Finite Difference Schemes: Methodology and Applications, World Scientific, Singapore, 2021.

[26] M.D.M. Hossain, A. Sultana, N. Purohit, Mental health outcomes of quarantine and isolation for infection prevention: a systematic umbrella review of the global evidence, Epidemiol. Health 42 (2020) (Mental health outcomes of quarantine & isolation).

[27] U.S. Department of Health and Human Services, What is the difference between isolation and quarantine? 2022, (Quarantine vs Isolation). (Accessed 19 May 2023).

[28] A. Dénes, A.B. Gumel, Modeling the impact of quarantine during an outbreak of Ebola virus disease, Infect. Dis. Model. 4 (2019) 12–27, (Ebola).

[29] W. Ahmad, M. Abbas, Effect of quarantine on transmission dynamics of Ebola virus epidemic: A mathematical analysis, Eur. Phys. J. Plus 136 (2021) 355, 1–33.

[30] D.J. Gerberry, F.A. Milner, An SEIQR model for childhood diseases, J. Math. Biol. 59 (2009) 535–561.

[31] A.B. Gumel, S. Ruan, T. Day, J. Watmough, F. Brauer, P. P. van den Driessche, et al., Modelling strategies for controlling SARS outbreaks, Proc. R. Soc. B 271 (2004) 2223–2232.

[32] P. Saha, S.K. Biswas, M.H.A. Biswas, U. Ghosh, An SEQAIHR model to study COVID-19 transmission and optimal control strategies in Hong Kong 2022, Nonlinear Dynam. 7 (2023) 6873–6893.

[33] F. Brauer, C. Castillo-Chavez, Mathematical Models in Population Biology and Epidemiology, Springer, New York Dordrecht Heidelberg London, 2012, pp. 377–378.

[34] A.B. Gumel, S. Ruan, T. Day, J. Watmough, F. Brauer, P. van den Driessche, et al., Modelling strategies for controlling SARS outbreaks, R. Soc. 271 (2004) 2223–2232.

[35] M. Lipsitch, T. Cohen, B. Cooper, J.M. Robins, S. Ma, L. James, et al., Transmission dynamics and control of severe acute respiratory syndrome, Science 30 (2003) 1966–1970.

[36] C.A. Zampieri, N.J. Sullivan, G.J. Nabel, Immunopathology of highly virulent pathogens: Insights from Ebola virus, Nature Immunol. 8 (2007) 1159–1164.

[37] A. Ball, Characterizing Protective Antibody Responses to Recombinant Ebola Virus Subunit Vaccines in Non-Human Primates (Ph.D. thesis), University of Hawai'i, Manoa, 2023.

[38] A. Brettin, R. Rossi-Goldthorpe, K. Weishaar, I.V. Erovenko, Ebola could be eradicated through voluntary vaccination, R. Soc. Open Sci. 5 (2017) 171591, 1–12.

[39] Z.-Q. Xia, S.-F. Wang, S.-L. Li, L.-Y. Huang, W.-Y. Zhang, G.-Q. Sun, et al., Modeling the transmission dynamics of Ebola virus disease in Liberia, Sci. Rep. 5 (2015) 13857, (Modeling the Transmission Dynamics of Ebola Virus Disease).

[40] D. Luo, R. Zheng, D. Wang, X. Zhang, Yi Yin, Kai Wang, et al., Effect of sexual transmission on the West Africa Ebola outbreak in 2014: a mathematical modelling study, Sci. Rep. 9 (2019) 1653, (Sexual transmission of Ebola).

[41] T.W. Tulu, B. Tian, Z. Wu, Modeling the effect of quarantine and vaccination on Ebola disease, Adv. Differerence Equ. 178 (2017) 1–14.

[42] Health24, Signs and symptoms of Ebola, 2014, (Ebola signs).

[43] V.P. Latha, F.A. Rihan, R. Rakkiyappan, A fractional-order delay differential model for Ebola infection and $CD8^+$ T-cells response: Stability analysis and Hopf bifurcation, Int. J. Biomath. 10 (2017) 1750111–1–22.

[44] N. Ahmed, M. Fatima, D. Baleanu, K.S. Nisar, I. Khan, M. Rafiq, et al., Numerical analysis of the susceptible exposed infected quarantined and vaccinated (SEIQV) reaction-diffusion epidemic model, Front. Phys. 7 (2020) 220, (A SEIQV Model).

[45] K.N. Nabi, Forecasting COVID-19 pandemic: A data-driven analysis, Chaos Solitons Fractals 139 (2020) 1–15.

[46] National Cancer Institute (NIH), Screening, 2023, (Patchy Environment). (Accessed 19 May 2023).

[47] I. Al-Darabsah, Y. Yuan, A time-delayed epidemic model for Ebola disease transmission, Appl. Math. Comput. 290 (2016) 307–325.

[48] C. Tadmon, J.N. Kengne, Mathematical modelling and nonstandard finite scheme analysis for an Ebola model transmission with information and voluntary isolation, J. Difference Equ. Appl. (2022) 1–37, http://dx.doi.org/10.1080/10236198.2022.2042524, (Ebola Model Transmission with Information and Voluntary Isolation).

[49] J. Arino, K. Khan, Using mathematical modeling to integrate disease surveillance and global air transportation data, in: D. Chen, B. Moulin, J. Wu (Eds.), Analyzing and Modeling Spatial and Temporal Dynamics of Infectious Diseases, in: Wiley Series in Probability and Statistics, John Wiley & Sons, New Jersey, 2015, pp. 97–108.

[50] F.B. Agusto, M.I. Teboh-Ewungkem, A.B. Gumel, Mathematical assessment of the effect of traditional beliefs and customs on the transmission dynamics of the 2014 Ebola outbreaks, BMC Med. 13 (2015) 96, 1–17.

[51] E. Grigorieva, E. Khailov, Determination of the optimal controls for an Ebola epidemic model, Discrete Contin. Dyn. Syst. Ser. B 11 (2018) 1071–1101.

[52] PopulationPyramid.net, Population pyramids of the world from 1950 to 2100, 2013, (Population Pyramids).

[53] Countryeconomy.com, Liberia-population, 2023, (Liberia-Population). (Accessed 26 April 2023).

[54] Macrotrends, Sierra Leone population 1950-2023, 2013, (Population). (Accessed 26 April 2023).

[55] WHO, Ebola data and statistics, 2015, (Ebola Statistics). (Accessed 22 August 2023).

[56] Jianquan Li, X. Wang, X. Lin, Impact of behavioural change on the epidemic characteristics of an epidemic model without vital dynamics, Math. Biosci. Eng. 15 (6) (2018) 1425–1434.

[57] E.A. Iboi, O. Sharomi, C.N. Ngonghala, A.B. Gumel, Mathematical modeling and analysis of COVID-19 pandemic in Nigeria, Math. Bioci. Eng. 17 (2020) 7192–7220.

[58] The World Bank, Death rate Crude (per 1 000people), 2022, (World Bank). Last access 30–08–2023.

[59] S. Merler, M. Ajelli, M. Fumanelli, L. Parlamento, S. Piontti, A.P.Y. Dean, et al., Containing Ebola at the source with ring vaccination, PLOS Negl. Trop. Dis. 10 (11) (2016) 1–11.

[60] C.M. Rivers, E.T. Lofgren, M. Marathe, S. Eubank, B.L. Lewis, Modelling the impact of interventions on an epidemic of Ebola in Sierra Leone and Liberia, PLOS Curr. Outbreaks (2014) (Epidemic of Ebola in Sierra Leone and Liberia).

[61] A. Rachab, A mathematical model with isolation for the dynamics of Ebola virus, J. Phys. Conf. Ser. 1132 (2018) (Mathematical model with isolation).

[62] A.M. Stuart, A.R. Humphries, Dynamical Systems and Numerical Analysis, Cambridge University Press, New York, 1998.

[63] S. Busenberg, K. Cooke, Vertically Transmitted Disease: Models and Dynamics, Springer Science & Business Media, New York, 1993.

[64] G. Sallet, Lecture Notes on Mathematical Epidemiology, University of Pretoria, 2018.

[65] Berman, Plemmons, Nonnegative Matrices in the Mathematical Sciences, Academic Press, New York, 1979.

[66] P. van den Driessche, J. Watmough, Reproduction numbers and sub-threshold endemic equilibria for compartment models of disease transmission, Math. Biosci. 180 (2002) 29–48.

[67] T.-T. Lu, S.-H. Shiou, Inverses of 2 ×2 block matrices, Comput. Math. Appl. 43 (2002) 119–129.

[68] C. Castillo-Chavez, Z. Feng, W. Huang, On the computation of $\mathcal{R}_0$ and its role on global stability, in: P.C. Castillo-Chavez, S. Blower, P. Driessche, D. Kirschner, A.-A. Yakubu (Eds.), Mathematical Approaches for Emerging and Reemerging Infectious Diseases: An Introduction, Vol. 125, Springer Science & Business Media, Berlin, 2002, pp. 229–250, ($R0$ role).

[69] R. Anguelov, J.M.-S. Lubuma, Contributions to the mathematics of the non-standard finite difference methods and applications, Numer. Methods Partial Differential Equations 17 (5) (2001) 518–543.

[70] T. Berge, J.M.-S. Lubuma, G.M. Moremedi, N. Morris, R. Kondera-Shava, A simple mathematical model for Ebola in Africa, J. Biol. Dyn. 11 (1) (2017) 42–74.

[71] N.L. Boddington, S. Steinberger, R.G. Pebody, Screening at ports of entry for Ebola Virus Disease in England-a descriptive analysis of screening assessment data, 2014–2015, J. Public Health 44 (2) (2022) 370–377.
[72] K. Wickramage, Airport entry and exit screening during the Ebola virus disease outbreak in Sierra Leone, 2014 to 2016, Biomed Res. Int. 2019 (2019) 3832790, (Entry & Exit Screening).
[73] WHO, Technical note for Ebola preparedness planning for entry screening at airports, ports and land crossings, 2014, (No entry screening recommendation).
[74] J.D. Kelly, S.D. Weiser, B. Wilson, et al., Ebola virus disease-related stigma among survivors declined in liberia over an 18-month, post-outbreak period: An observational cohort study, PLoS Negl. Trop. Dis. 13 (2) (2019) e0007185, (EVD-Related Stigma).
[75] K. Kupferschmidt, Ebola veteran promises an end to Congo's epidemic, 2019, Africa, Health. (Ending EVD).
[76] R.E. Mickens, Nonstandard Finite Difference Models of Differential Equations, World Scientific, Singapore, 1994.
[77] D.T. Dimitrov, H.V. Kojouharov, B.M. Chen-Charpentier, Reliable finite difference schemes with applications in mathematical biology, in: R.E. Mickens (Ed.), Advances in the Applications of Nonstandard Finite Difference Schemes, World Scientific, Singapore, 2005, pp. 249–285.
[78] R. Anguelov, T. Berge, M. Chapwanya, J.K. Djoko, P. Karma, J.M.-S. Lubuma, et al., Nonstandard finite difference method revisited and application to the Ebola virus disease transmission dynamics, J. Difference Equ. Appl. 26 (6) (2020) 818–854.